

SPEED AND POSITION SENSORLESS
PERMANENT MAGNET SYNCHRONOUS MOTOR DRIVES

CENTRE FOR NEWFOUNDLAND STUDIES

**TOTAL OF 10 PAGES ONLY
MAY BE XEROXED**

(Without Author's Permission)

M. ASHRAFUL HOQUE



**Speed and Position Sensorless
Permanent Magnet Synchronous Motor Drives**

By

©M. Ashraful Hoque

A thesis submitted to the School of Graduate Studies
in partial fulfillment of the requirements for the degree of
Master of Engineering

Faculty of Engineering and Applied Science
Memorial University of Newfoundland

August, 1993

St. John's

Newfoundland

Canada



National Library
of Canada

Acquisitions and
Bibliographic Services Branch

395 Wellington Street
Ottawa, Ontario
K1A 0N4

Bibliothèque nationale
du Canada

Direction des acquisitions et
des services bibliographiques

395, rue Wellington
Ottawa (Ontario)
K1A 0N4

Author's Note

Author's Note

The author has granted an irrevocable non-exclusive licence allowing the National Library of Canada to reproduce, loan, distribute or sell copies of his/her thesis by any means and in any form or format, making this thesis available to interested persons.

L'auteur a accordé une licence irrévocable et non exclusive permettant à la Bibliothèque nationale du Canada de reproduire, prêter, distribuer ou vendre des copies de sa thèse de quelque manière et sous quelque forme que ce soit pour mettre des exemplaires de cette thèse à la disposition des personnes intéressées.

The author retains ownership of the copyright in his/her thesis. Neither the thesis nor substantial extracts from it may be printed or otherwise reproduced without his/her permission.

L'auteur conserve la propriété du droit d'auteur qui protège sa thèse. Ni la thèse ni des extraits substantiels de celle-ci ne doivent être imprimés ou autrement reproduits sans son autorisation.

ISBN 0-315-86631-4

Canada

Abstract

DC motors have played a crucial role in drive technology during the last few decades of this century. Recent developments in power converters, digital signal processors and magnetic materials make it possible to use ac motors in a variety of drive applications. Permanent magnet synchronous (PMS) motors are gaining wide recognition over other types of motors in drive systems, mainly due to their inherently advantageous features. For successful operation of PMS motor drives, position and speed sensing are of critical importance. Conventional sensors are expensive and hamper sturdiness of industrial drives. Hence speed and position sensorless PMS drive draws wide attention. In this work, an algorithm is developed which enables the PMS drive to operate successfully at any speed (from zero to twice the rated value) without any mechanical speed and position sensors while keeping the maximum output voltage of the inverter constant above the base speed. New expressions have been derived for the rotor speed and position in terms of the stator voltages and currents. A method has also been suggested to calculate the input voltage of the motor. The present work is an attempt to provide theoretical analysis of speed and position sensorless PMS drives with computer simulations of various drive configurations. Experimental results which are in agreement with the proposed algorithm have been included.

Acknowledgments

I would like to express my sincerest gratitude and appreciation to my supervisor Professor M.Azizur Rahman for his guidance, advice and encouragement throughout my program. My sincerest thanks to Canadian International Development Agency (CIDA) for sponsoring the MUN/CIDA/BIT project which afforded me the opportunity to become involved with the program. I also thank Mr. Tony Williamson and Ms. M. Atkinson of Memorial University for their help in this project. Dr. C. Sharpe, Associate Dean of the School of Graduate Studies of Memorial University deserves special thanks for his support.

I acknowledge the assistance received from the faculty members, fellow graduate students and other staff members of the Faculty of Engineering and Applied Science.

Finally I express my sincere appreciation to my wife, our daughter as well as other family members and friends without whose support, encouragement and understanding, it would not have been possible to complete this work.

Contents

Abstract	ii
Acknowledgement	iii
Contents	iv
List of Figures	v
List of Tables	vi
List of Symbols	viii
1 Introduction	1
1.1 Brief review of motors in drive systems	2
1.2 Problem statement	4
1.3 Thesis organization	5
2 Literature Survey	6
2.0.1 Wave-form detection technique	9
2.0.2 Flux linkage method	15
2.0.3 Digital signal processor based rotor position estimation technique	16

2.0.1	Vector control of permanent magnet synchronous motor	19
2.1	Summary	22
3	Analysis	24
3.1	Relationship between winding inductances and voltages of a general synchronous machine	25
3.2	Machine equations for permanent magnet synchronous motor	35
3.3	Transformation of machine equations in synchronously rotating frames- Park's equations	36
3.3.1	General equations on transformation	36
3.3.2	Park's Equations	38
3.3.3	Relationship between orthogonal quantities of stationary reference frame and synchronously rotating reference frame	43
3.3.4	Relationship between three-phase and orthogonal quantities in stationary reference frame	46
3.4	Rotor speed and rotor-position in terms of stator currents and voltage	49
3.5	Summary	53
4	Simulation of position sensorless permanent magnet synchronous motor drive	54
4.1	Simulation of permanent magnet synchronous motor with sinusoidal supply without control scheme.	55
4.2	Simulation of closed loop vector control of permanent magnet synchronous motor	59
4.2.1	PMS motor drive system upto base speed with speed feedback loop only	61

4.2.2	Current controller and voltage source inverter (VSI)	64
4.2.3	Working principle of the drive system	68
4.3	PMS motor drive with two control loops	75
4.4	PMS motor drive operation above base speed-Field weakening method	81
4.5	Discussions on Simulated Results	89
5	Experimental Results	97
5.1	Determination of the magnet constant, λ_M	97
5.2	Verification of rotor position angle and speed using sensorless algorithm	99
5.3	Discussions on the experimental results	103
6	Conclusions	104
6.1	Recommendations for future research	105
	References	107
	Appendices	112
A	PMS motor design data	113
B	Experimental waveforms	114

List of Figures

2.1	Vector control of permanent magnet synchronous motor	7
2.2	Circuit for zero-crossing detection of back emf [6]	10
2.3	Phase inductance, phase voltage and phase current during probing of phase [16].	13
2.4	Rotor position estimation scheme by flux linkage method [19]	16
2.5	State space model of rotor position estimation	18
2.6	DSP based rotor position estimation	19
2.7	Vector control scheme of permanent magnet synchronous motor	22
3.1	Two pole, three phase, wye-connected, salient pole synchronous ma- chine [38]	26
3.2	Distribution of phase winding and corresponding MMF [38]	27
3.3	Park's model of permanent magnet synchronous motor: (a) d-axis (b) q-axis	42
3.4	(a) Co-ordinate systems of the stationary reference frame with an initial θ . (b) Co-ordinate systems of stationary reference frame with $\theta = 0$	46
4.1	Block diagram of open loop simulation of PMS motor	56
4.2	Flow chart for open loop simulation of PMS motor	57

4.3	Open loop simulation of PMS motor. (a) Rotor speed. (b) Rotor position angle.	58
4.4	(a) Vector diagram for drives upto base speed [41]. (b) Torque speed characteristics.	60
4.5	Block diagram of speed control loop drive system [39]	62
4.6	Voltage source inverter and current controller [39]	65
4.7	(a) Hysteresis current controller (b) Inverter output [39]	66
4.8	Flow chart of PMS motor drive with one feed back speed loop (upto base speed).	69
4.9	Simulation of single loop (speed loop) PMS motor drive. (a) Reference rotor speed. (b) Actual rotor speed.	71
4.10	Simulation of single loop (speed loop) PMS motor drive. (a) Rotor position (b) Unit vectors.	72
4.11	Simulation of single loop (speed loop) PMS motor drive. (a) Phase currents (b) Reference torque component current	73
4.12	Output voltage of the inverter	74
4.13	Block diagram of PMS motor drive system with two control loops. . .	76
4.14	Flow chart for the computer simulation of modified PMS motor drive. .	78
4.15	Simulation of two-loop (speed and torque) PMS motor drive. (a) Reference speed. (b) Actual speed.	79
4.16	Simulation of two-loop (speed and torque) PMS motor drive. (a) Rotor position angle. (b) Unit vectors.	80
4.17	Simulation of two-loop (speed and torque) PMS motor drive. (a) Phase currents. (b) Inverter output voltage.	81

4.18	Simulation of two-loop (speed and torque) PMS motor drive. (a) Reference torque. (b) Generated torque.	82
4.19	Simulation of two-loop (speed and torque) PMS motor drive. (a) Torque vs speed characteristics. (b) Voltage vs speed characteristics.	83
4.20	Vector diagram of PMS motor above base speed.	85
4.21	Block diagram of the PMS motor drive with field weakening feature.	86
4.22	Flow chart for the computer simulation of PMS motor drive-operated at any speed.	88
4.23	Simulation of general PMS drive operated at various speeds. (a) Reference speed. (b) Actual speed.	90
4.24	Simulation of general PMS drive operated at various speeds. (a) Rotor position. (b) Unit vectors.	91
4.25	Simulation of general PMS drive operated at various speeds. (a) Phase currents. (b) Peak voltage of the inverter.	92
4.26	Simulation of general PMS drive operated at various speeds. (a) Reference torque. (b) Generated torque.	93
4.27	Simulation of general PMS drive operated at various speeds. (a) Torque component current. (b) Demagnetizing current.	94
4.28	Simulation of general PMS drive operated at various speeds. (a) Torque vs speed characteristics. (b) Voltage vs speed characteristics.	95
5.1	Experimental set up for the determination of magnet constant λ_M	98
5.2	Experimental setup for the verification of sensorless algorithm of PMS motor.	100
5.3	Simulated and experimental results of open loop PMS motor: (a) Simulated rotor position angle (b) Experimental rotor position angle	102

List of Tables

5.1	Open circuit voltage and magnet constant at various speeds of PMS motor.	99
5.2	Simulation and experimental results of open loop PMS motor.	101
5.3	Simulation and experimental rotor position, θ_r of open loop PMS motor	101

Nomenclature

α_1, α_2	: constants used in minimum and maximum air-gap measurement
γ	: phase angle between voltage and current
θ_i	: rotor displacement
θ_{i0}	: initial rotor position angle
$\lambda_{sa}, \lambda_{sb}, \lambda_{sc}$: stator self flux linkages
λ_{ff}	: field self flux linkage
$\lambda_s, \lambda_b, \lambda_c$: total flux linkages in stator phases
λ_f	: total flux linkages in field
$[\lambda_F]$: flux linkage matrix of permanent magnet rotor
λ_M	: magnet constant
μ_0	: permeability for free space
μ_r	: relative permeability
ϕ_s	: stator displacement
ϕ_r	: relative displacement of rotor
ω_r	: rotor angular speed
i_a, i_b, i_c	: phase currents
i'_d, i'_q	: direct and quadrature axis currents in rotor reference frame
i_d, i_q	: direct and quadrature axis currents in stator reference frame
l	: length of air gap
p	: operator $\frac{d}{dt}$
r	: mean radius of air gap
r_a, r_b, r_c	: stator phase resistance
r_s	: stator phase resistance when considered equal

v_a, v_b, v_c	: phase voltages
v_d^r, v_q^r	: direct and quadrature axis voltages in rotor reference frame
v_d^s, v_q^s	: direct and quadrature axis voltages in stator reference frame
I_m	: peak value of input current of the motor
K_1, K_2, K_3, K_4	: PI: proportional integral controller constants
K_5	: integrator constant
$[L]$: inductance matrix
L_l	: stator leakage inductance
L_{aq}, L_{bb}, L_{cc}	: stator self inductances
L_{ff}	: field self inductance
L_{mq}	: q-axis mutual inductance
L_{md}	: d-axis mutual inductance
L_q	: q-axis inductance
L_d	: d-axis inductance
L_s	: static inductance
M_{ab}, M_{bc}, M_{ca}	: stator mutual inductances
M_{af}, M_{bf}, M_{cf}	: field mutual inductances
P	: Number of poles
V_b	: voltage induced by permanent magnet rotor
V_m	: peak value of input voltage of the motor
V_s	: applied voltage to motor terminal

Chapter 1

Introduction

With the advancement of technology, the areas of applications for electric motors increase in a versatile manner. Recent developments in magnetic materials, semiconductor and microprocessor technology have made revolutionary advancements on the design and control of electric motors. As a result, the use of conventional electric motors is becoming obsolete in modern drive system. For example, dc, ac induction, conventional wire-wound excited synchronous motor drives are being increasingly replaced by the permanent magnet synchronous motor (PMS motor) drives. The PMS motor has numerous advantages over other motors primarily due to the absence of commutator and also because it is not subject to the limitations of dc motors, (the limit on maximum voltage, maximum speed, maximum power, frequent maintenance, and inability to operate in explosive and contaminated environments). PMS motors can offer significantly higher advantages and efficiency over induction machines when employed in adjustable speed drives, because it does not have the slip losses as is the case with induction motors. PMS motors are superior to the conventional wire-wound excited synchronous motors because the field coil, dc supply and slip rings are eliminated in the former which results in low power loss and less complex motor drive

design. The control of PMS motors is done entirely through the stator, since there is no provision for rotor side excitation control. Vector control method is generally suggested for the variable speed PMS motor drives where the speed and rotor position information are used as the feedback control of the drives. Vector controlled PMS motor drive offers a number of attractive features such as smooth operations at a wide range of speeds, high torque capability, high efficiency along with a high power factor and compact drive design.

1.1 Brief review of motors in drive systems

In most modern drive systems, typically dc motors, ac induction and synchronous motors are widely used.

DC motors

DC motors used in drive technology offer various control features as motor speed and torque can be controlled separately by armature and field currents. However, the main limitations associated with the dc motors are due to the commutators and brushes. Because of mechanical friction between commutator and the brushes, these motors require regular maintenance and frequent replacement of brushes. Sparking is a common phenomenon at the brushes which limits the power rating of the motor and its use in explosive environments. Recently, electronically commutated ac permanent magnet synchronous motors known as brushless dc motors are replacing the conventional dc motors in drive systems. These are actually polyphase synchronous motor with permanent magnet rotor. The motors are excited by power converters utilizing thyristors or power transistors and shaft position encoders. One problem with these

motors is that the speed varies with load. However, suitable control features can be used to overcome this difficulty.

AC induction motors

AC induction motors are being widely employed in drive system due to the simplicity of construction, reliability of operation in all environments, availability of low cost power converters, digital control devices, etc. However, due to slip I^2R losses, the drive system is not as efficient as is expected. Additional power loss and torque pulsation are two major problems which arise in induction motor drives due to the higher harmonics originated from the power converter. Moreover, real time implementation of induction motor drive system requires sophisticated modeling and estimation of machine parameters with complex control circuitry.

Synchronous motors

Synchronous motors of wire-wound type are common in drive systems because the field current can be controlled from the rotor side. But due to the presence of the field coil, dc supply and slip rings, drives become bulky and less efficient. Due to the recent developments in permanent magnet materials technology, PMS motors are becoming increasingly popular in drive applications. These types of motors are not subject to the limitations of dc, ac induction and wire-wound excited synchronous motors as previously discussed. The field excitation of these motors is obtained by suitably mounting permanent magnet materials in the rotor. Ferrite and rare earth, Samarium Cobalt and Neodymium Boron Iron (NdBFe) magnets with linear magnetizing characteristics in the second quadrant are employed in the rotor. Ferrites are commonly used because of the low cost, but the rare earths and NdBFe permanent

magnet although very expensive, allow large reduction in weight and size, because of their large coercive force and high remnance. The another advantage of PMS motor is that it can be operated in an improved power factor mode with a resultant reduction in copper loss. The basic control strategy of the PMS motor drive is to operate the motor preferably at a constant flux below the base speed and at a reduced flux and constant terminal voltage above the base speed. In modern PMS drive systems, vector control method is used to control the speed and torque of the motor. In this control strategy, speed and rotor position information are used as feedback signals to generate the reference input for a current controller. To obtain the feature of voltage source and current source inverter simultaneously, a hysteresis current controller is suggested for use in the drive system. For low speed and constant torque operation, the inverter voltage is pulse width modulated and the air gap flux is maintained constant. In high speed or constant horse power operation, the inverter voltage is at its maximum and the regulation of the stator current and air-gap flux is lost. Field weakening method is used to achieve these characteristics above the base speed. Since nothing can be controlled from the rotor side of the PMS motor, a demagnetizing current is generated in the rotor reference frame axis in order to oppose the permanent magnet flux, so that the inverter output voltage remains at its ceiling value.

1.2 Problem statement

Vector control method has been proposed to control the PMS motor in this present work. Rotor speed and rotor position should be detected in this control strategy. Numerous methods are available in the literature regarding rotor speed and position detection. Direct rotor position detection technique is one such method. This tech

nique uses tacho-generators, Hall effect elements, optical or inductive coupling sensors, shaft mounted encoder or resolver. The use of these mechanical sensors makes the drive system bulky, less efficient and expensive. In some fields of application such as the submersible motor drive, these sensors are totally unsuitable for use. Thus an indirect method of rotor position detection which detects the rotor position and calculates the rotor speed from the stator variables (such as stator voltages, currents, flux linkages and stator inductances), is investigated for the vector control of PMS motor drives in this present research. In literature, this method of rotor position detection technique is known as sensorless rotor position detection.

1.3 Thesis organization

This thesis consists of six chapters: Chapter two provides the literature survey of sensorless rotor position estimation techniques and the PMS motor drive. Chapter three provides the theoretical analysis of PMS motor and derivation of sensorless rotor position formulae. Chapter four includes the simulation of position sensorless PMS motor drive for different configurations. Chapter five provides some experimental results. Chapter six includes conclusions and recommendations for further research.

Chapter 2

Literature Survey

DC motors have been widely used as variable speed drives because their flux and torque can be easily controlled by the field and armature current respectively. In recent years, however, these drives are being replaced by ac drives, as dc motors have certain disadvantages owing to their commutators and brushes which require periodic maintenance and even replacements.

In ac motor drives, two types of control are employed namely, scalar control and vector control. Scalar control relates only to the magnitude of a variable, and their command and feedback signals are dc quantities which are proportional to the respective variables. In this control strategy, both the torque and flux are functions of voltage and frequency. This coupling effect slows the response of the ac drives. On the other hand, vector control method displays excellent performance for variable speed ac drives particularly in the case of PMS motor employing modern static converters. In vector control, both the phase angle and the magnitude of the current has to be controlled, that is, the current vector has to be controlled. Vector control of PMS motor is implemented when the system variables are transformed to a synchronously rotating frame where sinusoidal variables appear as dc quantities. The basic control

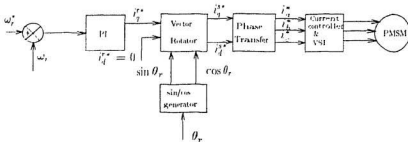


Figure 2.1: Vector control of permanent magnet synchronous motor

strategy is shown in Fig. 2.1. In this control scheme, the equivalent field current I_f of permanent magnet rotor is considered to be constant. The machine torque can be controlled with constant air gap flux by controlling the magnitude of quadrature axis current in rotor reference frame, i_q^r . From the block diagram it is seen that i_q^r can be formulated provided the rotor position is estimated. Numerous methods already exist in literature for the detection of rotor position. These can be categorized as direct position sensing and indirect position sensing. Conventional rotor position technique falls under direct position sensing method which is based on the use of tachogenerators, Hall effect elements, optical or inductive coupling sensors, shaft mounted encoders or resolvers. The use of these mechanical sensors makes drive systems complex and costly. In some areas of application such as in submersible motor drives, these types of position sensors are unsuitable. Thus indirect position detection technique has been investigated which replaces the mechanical sensors. This method of position detection is based on the measurement or identification of some electrical quantities of stator phase winding circuits, such as stator phase currents, voltages or inductances etc. which provide information about the position of the rotor at any

instant. This type of rotor position detection technique is known as the sensorless rotor position detection. Some well known and established sensorless rotor position detection techniques which already exist in literature are based on identifications or measurements or computations of stator variables. Among the widely accepted methods are rotor position estimation by wave-form detection technique, flux linkage method and computation based rotor position detection. In wave-form detection technique, some specific events of electrical quantities are identified such as maximum value or zero crossings in the wave-forms or changes in stator inductances which result due to consequences of the particular position of the rotor. These methods are simple and may be implemented using low cost electronic components. However, these methods are inaccurate, as all information are not available for detecting the position at various speeds of the motor. Flux linkage method is another rotor position detection technique where flux linkage is measured directly using sensing coils or estimated by integrating the phase voltage and compared with a reference flux linkage after which a decision is made regarding the commutation for a given value of current level.

Computation based rotor position estimations are becoming very popular because of recent developments in digital signal processor (dsp) and microprocessor technology. Highly complicated and time consuming calculations can be performed at high speeds using the digital signal processor. Thus, rotor position can be detected in real time by analyzing phase currents and voltages very conveniently. In particular, complex implementation of field oriented or vector control of ac drives where rotor position detection is necessary becomes an attractive feature when using this method. Computation based rotor position detection techniques can be categorized in two ways: observer based rotor position detection technique and direct computation based detection technique using digital signal processor. In observer based rotor

position detection technique, an observer is designed using estimated states such as two stator currents, rotor velocity and rotor position. A feedback loop is used to generate an error signal which is used in an iterative manner to correct the states of the system. Because of iteration, the whole system might be slow and complex. On the other hand, it is possible to use digital signal processor directly to detect the position of the rotor if the relation between the rotor position and the stator variables can be established. Thus the input of the processor would be currents and voltages while the output would be rotor position and rotor speed which can be used for the vector control of ac drives such as the permanent magnet synchronous motor drive.

The first part contains the critical review on the works of sensorless rotor position detection of ac motors and the second part contains the reviews on the vector control of ac drives.

2.0.1 Wave-form detection technique

This technique uses particular characteristics of electrical wave-form which are due to the position of the rotor. Detection of back emf and monitoring changes of inductances for the estimation of rotor position chiefly fall under this category.

Back emf method

This method considers that the phase commutation of a particular phase should occur when the back emf of that phase crosses the zero position. It can be mathematically shown that this zero-crossing point is achieved when the terminal voltage is equal to the neutral voltage. To obtain the correct signals for the bases of the transistor inverter it is necessary to delay this point by 90 electrical degrees. Firstly, the terminal voltages V_a , V_b , and V_c are converted to the triangular wave-forms through low pass

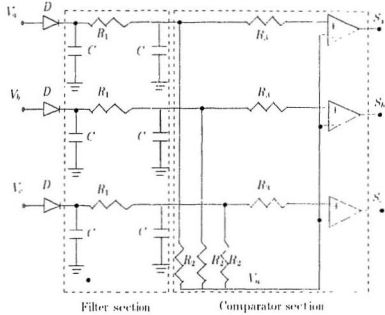


Figure 2.2: Circuit for zero-crossing detection of back emf [6]

filters as shown in Fig. 2.2. Then these voltages are shifted by 90 electrical degrees and compared with the neutral voltage V_a . Pulse signals S_a , S_b and S_c are produced by the comparators. Finally a microprocessor logically converts these pulses to six drive signals of the inverter. The performance of the whole drive system is quite satisfactory but the problem associated with it is the starting of the motor. A separate starting scheme is necessary for this type of position sensorless drive. Wave-form detection techniques incorporating back-emf for the estimation of rotor position for permanent magnet step motors are introduced by Kuo et al. [1]. This is the basic introductory paper where detailed mathematical models are proposed to present the

detection scheme. In particular, peaks of voltages across the live phases and zero crossing of back emf in the unenergized phases are sensed and information are obtained which are utilized for the detection of rotor position with the mathematical expressions presented. Hair [2] has reported an excellent feature of back emf (electromotive force) detection technique for a two phase stepping motors. The motor is operated with only one phase energised and the other phase is completely turned off and magnetically decoupled from the on-phase. The back emf of the off-phase is determined by measuring its open circuit voltage. Since the phase windings are physically 90 degrees apart, a simple sinusoidal back emf voltage is detected using the differential amplifier circuit. The rate of decay of current in off-phase must be sufficiently high to ensure that the zero crossing of the back emf can be detected. In some motors, particularly permanent magnet stepping motor driven by bipolar transistor drives, back emf cannot be detected directly because off winding is not available. Using analogue circuits for the reconstruction of back emf wave-form the phase voltages and currents, a method is suggested by Kuo & Butts [3] and Siefert [4] to control the phase excitation in such a motor. Antognini [5] has reported an alternative form of back emf reconstruction technique where time constant with and without back emf due to rotation has been compared and thus motional back emf is estimated for rotor position detection. Since data are digitally sampled, this method is relatively noise free. Iizuka et al. [6] have implemented microprocessor controlled sensorless brushless motor drives using the method that permits the determination of permanent magnet synchronous motor rotor position by the back emf induced in the stator winding. Their work experiences a setback because of the problem of starting. In another paper Antognini [7] has proposed a new way of monitoring the back emf of permanent magnet stepping motor and brushless dc motor with all phases energised

and full torque generated. In his work, he suggested that the phase windings be connected in such a way so that the generated back emf voltage difference in a pair of phase windings is not a function of phase current or phase impedance. Beverra et al. [8] have presented a method of rotor position detection by extracting information from rotor back emf for the permanent magnet synchronous motor. In their work, a six-switch full bridge inverter is used to detect the zero crossing of the back emf of the motor by exciting two phases of a wye connected motor at each time instant. The third unexcited winding has the infinite impedance and no current flows through it. On the other hand, back emf across the winding is easily detected. The position of the rotor can be estimated as the zero crossing of the back emf provides the necessary information.

All the techniques so far discussed have the major inherent drawback of low speed or standstill problems because back emf is *not* available or is noisy at these stages. Bahlmann [9] has suggested a suitable starting algorithm so that a considerable speed can be achieved for the determination of back emf.

Detection of rotor position by monitoring the changes of stator inductance

In this method of sensorless rotor position detection, one can use an inverter to probe the phase of an ac motor by alternate switching to generate the current pulses. The shapes of the current pulses are functions of phase inductance and hence motor position as shown in Fig. 2.3. A peak current pulse i_p is given by the following relationship:

$$i_p = \frac{VT}{L(\theta_p)} \quad (2.1)$$

where V is the inverter voltage, T is time period for which the phase is switched

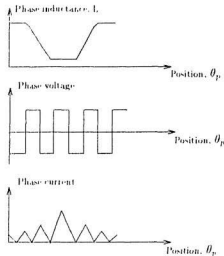


Figure 2.3: Phase inductance, phase voltage and phase current during probing of phase [16].

on, L is the phase inductance and θ_p is the rotor position at peak current. Since t_p is a measured quantity, θ_p can be determined from the knowledge of V , T and L . Hence, the stator winding inductance is a function of rotor position of permanent magnet motors. Researchers [10]-[12] have suggested a method of position detection technique by monitoring the phase current since the rate of change of current denotes the incremental change of rotor inductance which in turn dictates the position of the rotor. Frus and Kuo [13] have used the change of stator inductance for the estimation of rotor position of a single stack variable reluctance motor. They reported that the step of the motor is dictated by monitoring the currents of the independent phases since the phase currents change due to the changing nature of inductance of the sta-

tor. In another paper by Kno [14], detailed mathematical analysis of this method is given and it is suggested to monitor the current of the phase which has just been turned off and also that the maximum local value of this decaying current through the fly back circuit be observed. One important advantage of this method is that it is applicable to low speeds even at standstill where the back emf is insignificant. However, the relationship between the rate of change of current and rotor position becomes complicated because the incremental change of inductance depends on the phase current itself. Furthermore, the back emf affects the current at high speeds resulting in considerable error. Researchers have suggested a simple method of sensing inductance by pulsing a voltage on one of the off-phases and monitoring the resulting current ramps [15,16]. Current exceeds a threshold value when minimum inductance is approached. Thus a controller can be designed to switch the desired phases. By varying the threshold, the controller can precisely set the switching angle which results in a faster motor response. Ehsani et al. [17] have presented an alternative analogue technique incorporated with linear frequency modulated converter to measure the inductance of a non-conducting phase. In this paper, a frequency encoded signal is generated whose time period varies linearly with the phase inductance. The frequency encoded signal of the phase inductance can be decoded by microprocessors or any frequency-to-voltage converter circuit to obtain a voltage proportional to frequency. In a paper by Kulkarni and Ehsani [18], a novel position sensor elimination technique for interior permanent magnet synchronous motor drive is proposed. Using the knowledge of back emf, inductance is calculated. The calculated phase inductance is then used to estimate the rotor position with the help of a look up table. A scanning algorithm is used which searches for a value of phase inductance that is closest to the calculated value.

As mentioned previously, the method of rotor position detection by monitoring the change of stator inductance is not very reliable, because inductance variation is measured by measuring the change of stator current which in effect is not directly proportional to the stator inductance at any speed of operation due to the coupling effect of both and also because the back emf affects the phase current at high speeds.

2.0.2 Flux linkage method

Lyons et al. [19] have proposed a flux linkage estimation method to generate the phase commutation signal. Firstly a family of flux linkages Ψ vs currents I at various rotor positions are determined. Then these data are stored in a look-up table. The estimated flux linkage $\hat{\Psi}$ can be found from the following relationship using measured values of phase voltage and current.

$$\hat{\Psi} = \int (V - IR) \quad (2.2)$$

where V is the applied voltage and R the winding resistance. A reference value of flux linkage Ψ_r can be determined for a desired value of rotor position θ_r from the stored information with a known phase current I . A comparator as shown in Fig. 2-4 is used to compare the estimated and reference flux linkages. When the error $\Psi_e = \hat{\Psi} - \Psi_r = 0$ is obtained, it is concluded that the rotor is in the position of θ_r . However, this method suffers from measurement errors at the extreme angles of no-load and heavy-load conditions. Ertugrul and Acarnley [20] proposed an improved flux linkage method where the terminal voltage and line currents are used with the aim of estimating the winding flux linkages. At each time step, using previous predicted position information and the flux linkage value, the line current of the motor is esti-

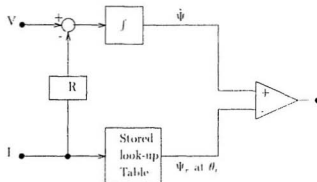


Figure 2.4: Rotor position estimation scheme by flux linkage method [19]

estimated in two stages to correct the predicted position and the estimated flux linkage respectively.

This method of rotor position estimation is preferable because it is capable of handling the feature at low speeds. But time consuming integration slows the process and hence is not suitable for fast response drives.

2.0.3 Digital signal processor based rotor position estimation technique

Observer based rotor position estimation and microprocessor or digital signal processor based rotor position detection fall under this category. In both cases, a large amount of mathematical calculations and computations are involved and hence the requirement for fast digital processors.

Observer based rotor position estimations

Okongwu, et al. [21] have developed a simple linear observer on linearized model of an ac machine where it is shown that the observer's performance is quite satisfactory for small perturbations about a wide range of operating points. Lumsdaine, et al. [22] have proposed an observer method for the variable reluctance motor where phase inductance variation effects fluxes in the phases have been taken into account. Lumsdaine and Lang [23] have proposed a state observer method which is driven by measurements of phase voltage and current for variable reluctance motor. A non-linear state observer technique is used by Dhaouadi et al. [24]. They have used the extended Kalman filter approach for the on-line estimation of the speed and rotor position by only using measurements of motor voltages and currents. This work is implemented with the fixed point digital signal processor TMS320C25. Greater accuracy can be achieved with the floating point digital signal processor. Jones and Lang [25] have proposed a rotor position detection technique based on state-space observer where mathematical model for state variables is done at first. After considering a number of factors which might lead to error, an observer is proposed which is non-linear in nature. The block diagram of a rotor position observer is shown in Fig. 2.5, where V_s , V_d , \hat{i}_d and \hat{i}_q are known quantities. This observer utilizes the $d-q$ transformation to obtain a corrective feedback which is dependent on error in both mechanical and electrical estimations, whereas only electrical variables are measured.

The main drawback of this observer based rotor position estimation technique is that it is very complex to implement in real time.

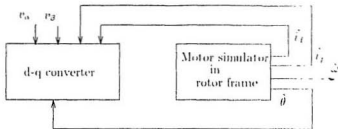


Figure 2.5: State-space model of rotor position estimation

Digital signal processor based rotor position estimation

Recent developments in digital signal processing and microprocessor based control tools have encouraged many researchers [26]-[32] to carry out works by analyzing and computing the real time variables as phase currents or phase voltages. Among them Matsui and Shigyo [27] have used the Texas Instrument digital signal processor for the intensive computations. The control strategy they considered is mainly based on voltage equations. The block diagram of this system configuration is given in Fig. 2.6. In this work, measured value of currents and computational values of voltages are used to estimate the rotor position (θ_a) which is then compared with a reference value of θ_a^* . The error is applied to proportional integral (PI) controllers and reference currents are produced accordingly. Comparing the reference currents with actual phase currents, desired pulse width modulated (PWM) voltages are generated using hysteresis current controllers. Rotor position estimation scheme of permanent magnet synchronous motors has been proposed by Naidu and Bose [31] using digital signal processors, but detailed implementation is absent in this report. Steingrimsen and Astrom [32] have proposed a digital signal processor implementation of a disk

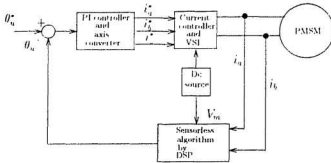


Figure 2.6: DSP based rotor position estimation

drive controller. In their work, the position information is obtained from a position detector which generates a voltage. The generated voltage is proportional to the mis-alignment of the head and track. A sensorless position detector is absent in this work.

After reviewing the above methods of rotor position detection, it seems that all methods with the exception of the digital signal processor based computational method of rotor position detection are either unsuitable for wide speed operation of ac motors, or give slow response or are very complex to implement in real time. Control of ac motors can be carried out at various speeds using the digital signal processor based computational method and no additional starting system is necessary.

2.0.4 Vector control of permanent magnet synchronous motor

As mentioned earlier, PMS motors can be controlled vectorically provided the position and speed of the rotor are determined. In the previous sections, works on the

sensorless rotor position detection were reviewed. In this section, works on vector control of different types of ac motors with and without position sensors has been reviewed and finally conclusion is made as to why computation based position sensorless algorithm is preferred for the control of permanent magnet synchronous motor drives. Lessmeier et al. [33] have compared the performance of synchronous motors and induction motors incorporating microprocessors. They have proposed the vector control strategy of ac motors in a synchronously rotating frame axis. Quadrature axis current has been identified as a control parameter up to base speed and after that an additional negative direct axis current is suggested to overcome the limitation of the maximum terminal voltage of the motor. Mechanical sensors have been used to detect the rotor position rather than the concept of sensorless operation of the motor. Kume and Iwakane [34] have presented a microprocessor based control scheme of ac motor drives. In this work, two closed control loops namely torque and speed loops are used to drive a PWM inverter. The authors have compared the test results of ac drives with dc drives and finally concluded that the performance of permanent magnet synchronous motor drives is as good as dc motor drives. Pillay et al. [35] have presented the vector and current controllers for permanent magnet synchronous motors. A resolver is proposed to sense the position of rotor which is analyzed by digital signal processor to give the position signal. This signal is compared with a reference to produce command speed, which is compared with the real speed and the error signal is used to produce reference currents. Using the current controller, drive signals of the inverter are generated. Texas Instrument digital signal processor is used in this work. Qian and Rahman [36] have reported a vector control strategy of permanent magnet hysteresis synchronous motor drives incorporating a microprocessor. In this control scheme, a tachometer is used to sense the speed which is fed to a \sin/\cos

generator to produce the direct and quadrature axis currents. The main control loop consists of two nested closed control loops. The inner loop is the fast response current loop with PD controllers and the slower outer loop is with PID controllers. Their simulated results have been verified experimentally. Matsui and Ohashi [26] have reported a digital signal processor based adaptive control of the brushless dc motor. In this work TMS320C25 Texas Instruments digital signal processor is used to implement the speed and current control scheme in real time. They have studied the effect of parameter variation on the performance of the drive. The important feature of their work is that the motor parameters used in the controller are identified at every sampling and so the control scheme is highly accurate. The sensors used for detecting the rotor position are mechanical. Bose and Szczesny [29] have shown simulated results of micro-computer based control of an interior permanent magnet synchronous machine. This drive system includes a constant torque region with zero speed operation and field weakening constant power regions at high speeds (above the base speed). The drive system is only designed with an outer torque control loop for a specific application like electric vehicle propulsion. General application is not possible with this type of drive as position and speed control loops are absent. In this drive system, an absolute shaft position encoder is proposed to detect the position of the rotor. Naidu and Bose [31] have simulated a position sensorless permanent magnet synchronous drive but their control system does not incorporate torque control loop and motor speed is limited up to the base speed.

A position sensorless permanent magnet synchronous motor drive can be implemented in the following way [37]: The block diagram of control scheme is shown in Fig. 2.7. In this work, two line-to-line voltages and two stator currents are sensed and processed in an analogue form to produce the stator flux linkage vector. These

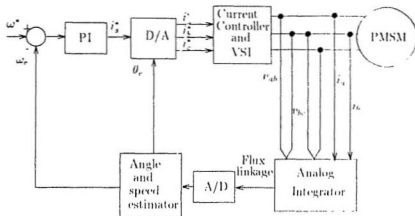


Figure 2.7: Vector control scheme of permanent magnet synchronous motor

flux linkages are processed and filtered to obtain information about rotor position θ and speed ω which are used to produce reference stator currents. The three phase currents sensed directly are compared with reference currents to drive a current controller which thus generates the drive signals for the inverter. Experimental results are provided for closed loop response to a step speed command. This is an excellent work for permanent magnet synchronous motor drives where the concept of position and speed sensorless operation is implemented. But this type of drive system always has the problem of starting. A separate starting strategy is introduced which makes the system complex.

2.1 Summary

In concluding this chapter it can be stated that there is a need to design a position sensorless permanent magnet drive which can be operated at any speed without any separate starting system. After reviewing works of rotor position estimation for vector controlled permanent magnet drives, computation based digital signal processor implemented rotor position detection technique is preferred for this present work because of the following reasons:

1. Drive can be operated at any speed without any additional starting circuit.
2. Because of inherent accuracy of the digital signal processor, the proposed drive would be very efficient.
3. Since complex mathematical calculations can be carried out by the digital signal processor within few nano seconds, fast response drive system is possible in this case.

Chapter 3

Analysis

PMS motors have the capability of high speed operation with high torque and offers smooth torque operation even at very low speeds. These characteristics of permanent magnet synchronous motors enable one to operate it in servo drive system along with the vector control scheme. The basic principle of vector control method is that it needs magnitude as well as angle information of controllable variables. Rotor position determines the angle of the variable and its detection is one of the basic requirements for this type of drive application. Numerous methods are found in literature for the detection of rotor position, but computation based sensorless rotor position detection technique is chosen for this present work because of its inherent accuracy and fast response characteristics when used with a special type of digital signal processor. A compact form of rotor position detection algorithm is possible for vector controlled permanent magnet synchronous motor drives when the motor is modelled in a synchronously rotating reference frame or when the machine equations are expressed in Park's transformation. In order to do so, the following steps have been taken.

- Relationship between machine inductance and voltage is established for synchronous machines in general.
- Voltage equations are formed in machine variables for permanent magnet synchronous machine variables.
- Reference frame theory is applied to transfer the machine equations from stationary frame axis with stator variables to synchronously rotating reference frame.
- Equations relating to rotor position detection are derived using the machine model in synchronously rotating frame.

3.1 Relationship between winding inductances and voltages of a general synchronous machine

A two pole, three phase, wye-connected, salient pole machine is chosen for this analysis as shown in Fig. 3.1. If $(\alpha_1 + \alpha_2)^{-1}$ and $(\alpha_1 - \alpha_2)^{-1}$ are taken as minimum and maximum air gap length, then the air gap is approximated by [38]

$$g(\phi_r) = \frac{1}{\alpha_1 - \alpha_2 \cos(2\phi_r)} \quad (3.1)$$

but since

$$\phi_s = (\phi_r + \theta_r) \quad (3.2)$$

Then it can be written that

$$g(\phi_s - \theta_r) = \frac{1}{\alpha_1 - \alpha_2 \cos 2(\phi_s - \theta_r)} \quad (3.3)$$

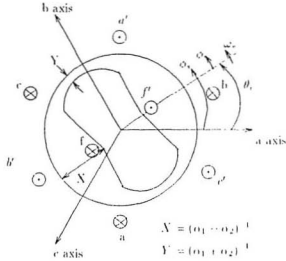


Figure 3.1: Two pole, three phase, wye-connected, salient pole synchronous machine [38]

where ϕ_s is the angular displacement of the stator, and θ_r is the angular displacement of rotor as shown in Fig 3.1. The air gap magneto-motive force can be expressed as:

$$MMF = H \times g = \frac{B_r}{\mu_r \mu_0} g \quad (3.1)$$

where H is the magnetic field intensity, B_r is the magnetic flux density and μ_0 is the permeability of free space and is given by $4\pi \times 10^{-7}$ and μ_r is the relative permeability (for permanent magnet, $\mu_r = 1.1$). Since the MMF is a function of ϕ_s , equation (3.1) can be modified to

$$B_r(\phi_s, \theta_r) = \mu_0 \mu_r \frac{MMF(\phi_s)}{g(\phi_s - \theta_r)} \quad (3.2)$$

If it is assumed that current is flowing only in phase a , then flux density due to this

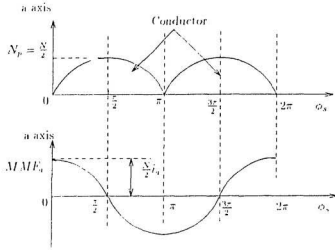


Figure 3.2: Distribution of phase winding and corresponding MMF [38]

is given by

$$B_r(\phi_s, \theta_r) = \mu_0 \mu_r \frac{MMF_{as}(\phi_s)}{g(\phi_s - \theta_r)} \quad (3.6)$$

The MMF due to current in a phase can be determined by analyzing Fig. 3.2. The suffix s stands for the stator quantity and is not repeated in the remaining text for the sake of simplicity. The winding distribution is taken as sinusoidal which is expressed for stator- a phase as

$$N_s = N_p \sin \phi_s, \quad 0 \leq \phi_s \leq \pi \quad (3.7)$$

$$N_s = -N_p \sin \phi_s, \quad \pi \leq \phi_s \leq 2\pi \quad (3.8)$$

where N_p is the maximum number of turns expressed in turns/radian. If N is considered as the number of turns of equivalent sinusoidally distributed winding in each

phase of the stator, then

$$N = \int_0^\pi N_p \sin \phi \, d\phi = 2N_p \quad (3.9)$$

Therefore,

$$N_p = \frac{N}{2} \quad (3.10)$$

Now it is assumed that the field winding is sinusoidally distributed with N_f equivalent turns as:

$$N_f(\phi_r) = \frac{N_f}{2} \cos \phi_r \quad (3.11)$$

Thus the air-gap MMF due to field current i_f in the rotor winding, can be expressed as

$$MMF_f = -\frac{N_f}{2} i_f \sin \phi_r \quad (3.12)$$

Hence the air-gap flux density due to field winding can be found by substituting equations (3.3) and (3.12) in equation (3.4) as:

$$B_r(\phi_r) = -\mu_0 \mu_r i_f \frac{N_f}{2} \sin \phi_r (\alpha_1 - \alpha_2 \cos(2\phi_r)) \quad (3.13)$$

If the air-gap flux distribution in stator is considered as sinusoidal, then its distribution in phase a winding can be determined from Fig. 3.2 and can be written as

$$MMF_a = \frac{N}{2} i_a \cos \phi \quad (3.14)$$

Similarly for the other two phases b and c it can be written that

$$MMF_b = \frac{N}{2} i_b \cos \left(\phi - \frac{2\pi}{3} \right) \quad (3.15)$$

$$MMF_c = \frac{N}{2} i_c \cos \left(\phi + \frac{2\pi}{3} \right) \quad (3.16)$$

Substituting equations (3.3) and (3.1) in equation (3.5), the expression of flux density due to current only in phase a becomes

$$B_r(\phi, \theta_r) = \mu_0 \mu_r \frac{N}{2} i_a \cos \phi [\alpha_1 - \alpha_2 \cos 2(\phi - \theta_r)] \quad (3.17)$$

Similarly, the flux densities for current in phase b and c , respectively are given as:

$$B_r(\phi, \theta_r) = \mu_0 \mu_r \frac{N}{2} i_b \cos \left(\phi - \frac{2\pi}{3} \right) [\alpha_1 - \alpha_2 \cos 2(\phi - \theta_r)] \quad (3.18)$$

$$B_r(\phi, \theta_r) = \mu_0 \mu_r \frac{N}{2} i_c \cos \left(\phi + \frac{2\pi}{3} \right) [\alpha_1 - \alpha_2 \cos 2(\phi - \theta_r)] \quad (3.19)$$

If the rotor winding is assumed to be sinusoidally distributed, then the rotor magnetomotive force can be expressed as

$$MMF_f = -\frac{N_f}{2} i_f \sin \phi_r \quad (3.20)$$

where N_f is the number of turns in equivalent sinusoidally distributed winding and i_f is the rotor current. Therefore, air-gap flux density due to current only in the rotor can be expressed in a similar way as the current in stator winding and is given by

$$B_r(\phi_r) = \mu_0 \mu_r \frac{N_f}{2} i_f \sin \phi_r (\alpha_1 - \alpha_2 \cos (2\phi_r)) \quad (3.21)$$

The flux linkage of a single turn of stator winding, located ϕ angle apart from a axis and whose span length is π radian is given by

$$\Phi(\phi, \theta_r) = \int_{\phi}^{\phi+\pi} B_r(\zeta, \theta_r) r l d\zeta \quad (3.22)$$

where l is the axial length of air gap of the machine, r is the mean radius of air gap and ζ is a dummy variable. Now the flux linkage in phase a due to current only through this winding becomes:

$$\lambda_{ia} = L_i i_a + \int N_a(\phi) \Phi(\phi, \theta_r) d\phi \quad (3.23)$$

Therefore, substituting equation (3.22) in (3.23), one obtains

$$\lambda_{ia} = L_i i_a + \int_{\phi} N_i(\phi) \int_{\phi}^{\phi+\pi} B_r(\zeta, \theta_r) r l \, d\zeta d\phi \quad (3.24)$$

where L_i is the stator leakage inductance due to leakage flux at the end turns. Now with the value of N_i and $B_r(\phi, \theta_r)$ of equations (3.7), (3.10) and (3.17) the expression for λ_{a3} becomes

$$\begin{aligned} \lambda_{a3} &= L_i i_a - \int_{\pi}^{2\pi} \sin \phi \int_{\phi}^{\phi+\pi} \mu_0 \mu_r \frac{N}{2} i_a \cos \zeta \{ \alpha_1 - \alpha_2 \cos 2(\zeta - \theta_r) \} r l \, d\zeta d\phi \\ &= L_i i_a + \left(\frac{N^2}{4} \right) \mu_0 \mu_r r l \int_{\pi}^{2\pi} \sin \phi \{ -2\alpha_1 \sin \phi \\ &\quad + \alpha_2 \cos 2\theta_r \{ \sin \phi + \frac{1}{3} \sin 3\phi \} - \alpha_2 \sin 2\theta_r \{ \cos \phi + \frac{1}{3} \cos 3\phi \} \} d\phi \\ &= L_i i_a + \frac{N^2}{4} \pi \mu_0 \mu_r r l \left(\alpha_1 - \frac{\alpha_2}{2} \cos 2\theta_r \right) i_a \end{aligned} \quad (3.25)$$

where ζ is used as a dummy variable for the purpose of integration. Recalling the definition of self inductance of a magnetically linear system as the ratio of flux linked by a winding to the current flowing in that winding with the absence of all other winding currents, the self inductance of a winding is given as

$$\begin{aligned} L_{aa} &= \frac{\lambda_{aa}}{i_a} \\ &= L_i + \frac{N^2}{4} \pi \mu_0 \mu_r r l \left(\alpha_1 - \frac{\alpha_2}{2} \cos 2\theta_r \right) \end{aligned} \quad (3.26)$$

Similarly, the self inductances of the other two windings, (b and c) can be found to be

$$L_{bb} = L_i + \frac{N^2}{4} \pi \mu_0 \mu_r r l \left[\alpha_1 - \frac{\alpha_2}{2} \cos 2 \left(\theta_r - \frac{2\pi}{3} \right) \right] \quad (3.27)$$

$$L_{cc} = L_i + \frac{N^2}{4} \pi \mu_0 \mu_r r l \left[\alpha_1 - \frac{\alpha_2}{2} \cos 2 \left(\theta_r + \frac{2\pi}{3} \right) \right] \quad (3.28)$$

The mutual flux linkage in a winding due to current in b winding is found in a similar manner, but in this case, the flux density will be taken due to i_b and can be written

as

$$\begin{aligned}
\lambda_{qb} &= \int N_q(\phi) \int_{\phi}^{\phi+\tau} B_r(\zeta, \theta_r) r l \, d\zeta d\phi \\
&= - \int_{\pi}^{2\pi} \frac{N}{2} \sin \phi \int_{\phi}^{\phi+\tau} \mu_0 \mu_r \frac{N}{2} i_b \cos(\zeta - \frac{2\pi}{3}) \\
&\quad [\alpha_1 - \alpha_2 \cos 2(\zeta - \theta_r)] r \, l \, d\zeta d\phi \\
&= - \frac{N^2}{4} \frac{\pi}{2} \mu_0 \mu_r r l \left[\alpha_1 + \alpha_2 \cos 2(\theta_r - \frac{\pi}{3}) \right] i_b
\end{aligned} \tag{3.29}$$

Thus the mutual inductance M_{qb} can be found using

$$\begin{aligned}
M_{qb} &= \frac{\lambda_{qb}}{i_b} \\
&= - \frac{N^2}{4} \frac{\pi}{2} \mu_0 \mu_r r l \left[\alpha_1 + \alpha_2 \cos 2(\theta_r - \frac{\pi}{3}) \right]
\end{aligned} \tag{3.30}$$

The mutual inductance M_{af} between the field winding and the stator phase a can be found similarly by:

$$M_{af} = \frac{NN_f}{4} \pi \mu_0 \mu_r r l \left(\alpha_1 + \frac{\alpha_2}{2} \right) \sin \theta_r \tag{3.31}$$

In a like manner, the mutual inductances between the different windings can be written as:

$$M_a = - \frac{N^2}{4} \frac{\pi}{2} \mu_0 \mu_r r l \left[\alpha_1 + \alpha_2 \cos 2 \left(\theta_r + \frac{\pi}{3} \right) \right] \tag{3.32}$$

$$M_b = - \frac{N^2}{4} \frac{\pi}{2} \mu_0 \mu_r r l [\alpha_1 + \alpha_2 \cos 2(\theta_r + \pi)] \tag{3.33}$$

$$M_{bf} = \frac{NN_f}{4} \pi \mu_0 \mu_r r l \left(\alpha_1 + \frac{\alpha_2}{2} \right) \sin \left(\theta_r - \frac{2\pi}{3} \right) \tag{3.34}$$

$$M_{cf} = \frac{NN_f}{4} \pi \mu_0 \mu_r r l \left(\alpha_1 + \frac{\alpha_2}{2} \right) \sin \left(\theta_r + \frac{2\pi}{3} \right) \tag{3.35}$$

The self flux linkage in the field winding can be found using

$$\lambda_{ff} = L_{ff} i_f + \int N_f(\phi_r) \Phi(\phi_r) d\phi_r \tag{3.36}$$

where $\Phi(\phi_r)$ is the flux due to field current and is given by equation (3.22)

$$\Phi(\phi_r) = \int_{\phi_r}^{\phi_r+\pi} B_r(\zeta) r l d\zeta \quad (3.37)$$

Now substituting the values of $N_f(\phi_r)$ and $\Phi(\phi_r)$ from equations (3.11) and (3.37) in equation (3.36) one obtains

$$\begin{aligned} \lambda_{ff} &= L_{lf} i_f + \int_{\frac{\pi}{2}}^{\frac{3\pi}{2}} \frac{N_f}{2} \cos \phi_r \\ &\quad \times \int_{\phi_r}^{\phi_r+\pi} \mu_0 \mu_r \frac{N_f}{2} \sin \zeta (\alpha_1 - \alpha_2 \cos 2\zeta) r l d\zeta d\phi_r \end{aligned} \quad (3.38)$$

After some trigonometric manipulations and necessary integrations, the self flux linkage of field winding due to the current through it, is given by

$$\lambda_{ff} = L_{lf} i_f + \frac{N_f^2}{4} \pi \mu_0 \mu_r r l \left(\alpha_1 + \frac{\alpha_2}{2} \right) i_f \quad (3.39)$$

Therefore, the self inductance of field winding is

$$\begin{aligned} L_{ff} &= \frac{\lambda_{ff}}{i_f} \\ &= L_{lf} + \frac{N_f^2}{4} \pi \mu_0 \mu_r r l \left(\alpha_1 + \frac{\alpha_2}{2} \right) \end{aligned} \quad (3.40)$$

where L_{lf} is the leakage inductance of the field winding. The inductances in different phase windings can be summarized by defining the following as

$$L_A = \frac{N^2}{4} \pi \mu_0 \mu_r r l \alpha_1 \quad (3.41)$$

$$L_B = \frac{1}{2} \frac{N^2}{4} \pi \mu_0 \mu_r r l \alpha_2 \quad (3.42)$$

$$M_f = \frac{N}{2} \frac{N_f}{2} \pi \mu_0 \mu_r r l \left(\alpha_1 + \frac{\alpha_2}{2} \right) \quad (3.43)$$

$$L_f = \frac{N_f^2}{4} \pi \mu_0 \mu_r r l \left(\alpha_1 + \frac{\alpha_2}{2} \right) \quad (3.44)$$

The machine inductances can now be expressed as

$$L_{aa} = L_l + L_A - L_B \cos 2\theta_r \quad (3.45)$$

$$L_{bb} = L_l + L_A - L_B \cos 2 \left(\theta_r - \frac{2\pi}{3} \right) \quad (3.46)$$

$$L_{cc} = L_l + L_A - L_B \cos 2 \left(\theta_r + \frac{2\pi}{3} \right) \quad (3.47)$$

$$L_{ff} = L_{lf} + L_f \quad (3.48)$$

$$M_{ab} = -\frac{1}{2} L_A - L_B \cos 2 \left(\theta_r - \frac{\pi}{3} \right) \quad (3.49)$$

$$M_{ac} = -\frac{1}{2} L_A - L_B \cos 2 \left(\theta_r + \frac{\pi}{3} \right) \quad (3.50)$$

$$M_{bc} = -\frac{1}{2} L_A - L_B \cos 2(\theta_r + \pi) \quad (3.51)$$

$$M_{af} = M_f \sin \theta_r \quad (3.52)$$

$$M_{bf} = M_f \sin \left(\theta_r - \frac{2\pi}{3} \right) \quad (3.53)$$

$$M_{cf} = M_f \sin \left(\theta_r + \frac{2\pi}{3} \right) \quad (3.54)$$

Thus the three phase inductances can be written in matrix form as:

$$[L] = \begin{bmatrix} L_{aa} & M_{ab} & M_{ac} \\ M_{ba} & L_{bb} & M_{bc} \\ M_{ca} & M_{cb} & L_{cc} \end{bmatrix} \quad (3.55)$$

Since

$$M_{ab} = M_{ba}, \quad M_{ac} = M_{ca}, \quad M_{bc} = M_{cb}$$

substituting equations (3.45)-(3.51) in equation (3.55), one gets

$$[L] = \begin{bmatrix} L_l + L_A - L_B \cos 2\theta_r & -\frac{1}{2}L_A - L_B \cos 2(\theta_r - \frac{\pi}{6}) & -\frac{1}{2}L_A - L_B \cos 2(\theta_r + \frac{\pi}{6}) \\ -\frac{1}{2}L_A - L_B \cos 2(\theta_r - \frac{\pi}{6}) & L_l + L_A - L_B \cos 2(\theta_r - \frac{\pi}{6}) & -\frac{1}{2}L_A - L_B \cos 2(\theta_r + \frac{\pi}{6}) \\ -\frac{1}{2}L_A - L_B \cos 2(\theta_r + \frac{\pi}{6}) & -\frac{1}{2}L_A - L_B \cos 2(\theta_r + \frac{\pi}{6}) & L_l + L_A - L_B \cos 2(\theta_r + \frac{\pi}{6}) \end{bmatrix} \quad (3.56)$$

Now the flux linkage in any winding is the summation of its self inductances and mutual inductances due to other currents. Hence the flux linkages in phase a , b and c and the field are given as:

$$\lambda_a = L_{aa}i_a + M_{ab}i_b + M_{ac}i_c + M_{af}i_f \quad (3.57)$$

$$\lambda_b = M_{ba}i_a + L_{bb}i_b + M_{bc}i_c + M_{bf}i_f \quad (3.58)$$

$$\lambda_c = M_{ca}i_a + M_{cb}i_b + L_{cc}i_c + M_{cf}i_f \quad (3.59)$$

$$\lambda_f = M_{fa}i_a + M_{fb}i_b + M_{fc}i_c + L_{ff}i_f \quad (3.60)$$

So the voltage equations for the elementary wire-wound excited synchronous machine can be written as

$$v_a = r_a i_a + \frac{d\lambda_a}{dt} \quad (3.61)$$

$$v_b = r_b i_b + \frac{d\lambda_b}{dt} \quad (3.62)$$

$$v_c = r_c i_c + \frac{d\lambda_c}{dt} \quad (3.63)$$

$$v_f = r_f i_f + \frac{d\lambda_f}{dt} \quad (3.64)$$

where r_a, r_b and r_c are the stator phase resistances and r_f is the rotor field resistance. These equations are valid for generalized machines with wire-wound excitation. The next step is to modify the above machine equations for a permanent magnet synchronous motor.

3.2 Machine equations for permanent magnet synchronous motor

The PMS motor is the same as the field-excited synchronous motor from the analytical view point. The only exception is that the rotor field excitation is replaced by a permanent magnet, which gives a constant flux λ_M . Now the flux linkage in the different stator phase windings due to permanent magnet rotor is given in matrix form as:

$$[\lambda_F] = \begin{bmatrix} \lambda_{af} \\ \lambda_{bf} \\ \lambda_{cf} \end{bmatrix} = \begin{bmatrix} \lambda_M \sin \theta_r \\ \lambda_M \sin \left(\theta_r - \frac{2\pi}{3} \right) \\ \lambda_M \sin \left(\theta_r + \frac{2\pi}{3} \right) \end{bmatrix} \quad (3.65)$$

So the flux linkage equations (3.57)-(3.59) are modified as

$$\lambda_a = L_{aa}i_a + M_{ab}i_b + M_{ac}i_c + \lambda_{af} \sin \theta_r \quad (3.66)$$

$$\lambda_b = M_{ba}i_a + L_{bb}i_b + M_{bc}i_c + \lambda_{bf} \sin \left(\theta_r - \frac{2\pi}{3} \right) \quad (3.67)$$

$$\lambda_c = M_{ca}i_a + M_{cb}i_b + L_{cc}i_c + \lambda_{cf} \sin \left(\theta_r + \frac{2\pi}{3} \right) \quad (3.68)$$

In matrix form one can write the above equations as

$$\begin{bmatrix} \lambda_a \\ \lambda_b \\ \lambda_c \end{bmatrix} = \begin{bmatrix} L_{aa} & M_{ab} & M_{ac} \\ L_{ba} & L_{bb} & L_{bc} \\ L_{ca} & L_{cb} & L_{cc} \end{bmatrix} \begin{bmatrix} i_a \\ i_b \\ i_c \end{bmatrix} + \lambda_M \begin{bmatrix} \sin \theta_r \\ \sin \theta_r - \frac{2\pi}{3} \\ \sin \theta_r + \frac{2\pi}{3} \end{bmatrix} \quad (3.69)$$

or, one can write the above equation in a more compact way as:

$$[\lambda_{ab}] = [L][i_{abc}] + [\lambda_F] \quad (3.70)$$

where the matrices $[L]$ and $[\lambda_F]$ are defined in equations (3.56) and (3.65), respectively.

Now, the voltage equations for the PMS machine can be written as:

$$v_a = r_a i_a + \frac{d\lambda_a}{dt} \quad (3.71)$$

$$v_b = r_b i_b + \frac{d\lambda_b}{dt} \quad (3.72)$$

$$v_a = r_c i_c + \frac{d\lambda_c}{dt} \quad (3.73)$$

or in matrix form

$$\begin{bmatrix} v_a \\ v_b \\ v_c \end{bmatrix} = \begin{bmatrix} r_a & 0 & 0 \\ 0 & r_b & 0 \\ 0 & 0 & r_c \end{bmatrix} \begin{bmatrix} i_a \\ i_b \\ i_c \end{bmatrix} + p \begin{bmatrix} \lambda_a \\ \lambda_b \\ \lambda_c \end{bmatrix} \quad (3.74)$$

One can write the above equation in compact form as:

$$[v_{abc}] = [r_{abc}][i_{abc}] + p[\lambda_{abc}] \quad (3.75)$$

where p is the operator defined as $p = \frac{d}{dt}$. In these voltage equations the flux linkage component contains inductances which are functions of rotor position θ_r , and the coefficients of the differential voltage equations are time varying except when the speed of the machine is zero. This makes analysis very complex unless all equations are transformed to the synchronously rotating frame where the machine inductances will no longer be dependent on rotor position. The machine equations in synchronously rotating frame are known as Park's equation.

3.3 Transformation of machine equations in synchronously rotating frame-Park's equations

3.3.1 General equations on transformation

In general, 3-phase variables in any reference frame can be transformed to the orthogonal components by the following relationship [38]:

$$[x_{qdo}] = [C_s][x_{abc}] \quad (3.76)$$

where

$$[x_{qdr}] = \begin{bmatrix} x_q \\ x_d \\ x_0 \end{bmatrix} \quad (3.77)$$

is the orthogonal components matrix transformed from three phase variables and

$$[x_{abc}] = \begin{bmatrix} x_a \\ x_b \\ x_c \end{bmatrix} \quad (3.78)$$

is the matrix for three phase variables in any reference frame and

$$[C_1] = \frac{2}{3} \begin{bmatrix} \cos \theta & \cos(\theta - \frac{2\pi}{3}) & \cos(\theta + \frac{2\pi}{3}) \\ \sin \theta & \sin(\theta - \frac{2\pi}{3}) & \sin(\theta + \frac{2\pi}{3}) \\ \frac{1}{2} & \frac{1}{2} & \frac{1}{2} \end{bmatrix} \quad (3.79)$$

is the co-efficient matrix of transformation, where

$$\theta = \int_0^t \omega(\eta) d\eta + \theta(0) \quad (3.80)$$

Here η is the dummy variable of integration and $\theta(0)$ is the angle difference between axes of transformation at $t = 0$ and ω is the speed of the transformed axis. The inverse of $[C_1]$ is given by the following equation:

$$[C_1]^{-1} = \begin{bmatrix} \cos \theta & \sin \theta & 1 \\ \cos(\theta - \frac{2\pi}{3}) & \sin(\theta - \frac{2\pi}{3}) & 1 \\ \cos(\theta + \frac{2\pi}{3}) & \sin(\theta + \frac{2\pi}{3}) & 1 \end{bmatrix} \quad (3.81)$$

In equations (3.76)-(3.78), x can represent any variable such as voltage, current or flux linkage.

3.3.2 Park's Equations

Park's equations in machine variables can be achieved by transforming the equations of the stationary axis to a synchronously rotating frame axis. Starting with the equations described in section (3.3.1), the only modification is that 'r' is taken as the superscript or subscripts with the variables to represent that the transformation is taking place to the rotating frame axis. Thus equations (3.79), (3.80) and (3.81) are modified as follows:

$$[C_2] = \frac{2}{3} \begin{bmatrix} \cos \theta_r & \cos(\theta_r - \frac{2\pi}{3}) & \cos(\theta_r + \frac{2\pi}{3}) \\ \sin \theta_r & \sin(\theta_r - \frac{2\pi}{3}) & \sin(\theta_r + \frac{2\pi}{3}) \\ \frac{1}{2} & \frac{1}{2} & \frac{1}{2} \end{bmatrix} \quad (3.82)$$

$$\theta_r = \int_0^t \omega_r(\eta) d\eta + \theta_r(0) \quad (3.83)$$

and the inverse of the above matrix can be found as:

$$[C_2]^{-1} = \begin{bmatrix} \cos \theta_r & \sin \theta_r & 1 \\ \cos(\theta_r - \frac{2\pi}{3}) & \sin(\theta_r - \frac{2\pi}{3}) & 1 \\ \cos(\theta_r + \frac{2\pi}{3}) & \sin(\theta_r + \frac{2\pi}{3}) & 1 \end{bmatrix} \quad (3.84)$$

The voltage equations in a stationary reference frame can be transformed to the orthogonal components of a rotating reference frame as:

$$[v_{r\theta 0}^r] = [C_2][v_{abc}] \quad (3.85)$$

Now substituting equation (3.75) in equation (3.85) yields

$$[v_{r\theta 0}^r] = [C_2]\{[v_{abc}][i_{abc}] + p[\lambda_{abc}]\} \quad (3.86)$$

But since it can be written that

$$[v_{r\theta 0}^r] = [C_2][i_{abc}] \quad (3.87)$$

$$[r_{qb}] = [C_2]^{-1}[\lambda_{qb}^r] \quad (3.88)$$

$$[\lambda_{abc}] = [C_2]^{-1}[\lambda_{qbm}^r] \quad (3.89)$$

Substituting equation (3.87) and (3.89) in (3.86) one gets,

$$\begin{aligned} [v_{qb}] &= [C_2]\{[r_{abc}][C_2]^{-1}[\lambda_{qb}^r] + p[C_2]^{-1}[\lambda_{qbm}^r]\} \\ &= [C_2][r_{abc}][C_2]^{-1} + [C_2]p[C_2]^{-1}[\lambda_{qbm}^r] + [C_2][C_2]^{-1}p[\lambda_{qbm}^r] \end{aligned} \quad (3.90)$$

Now $[C_2][r_{abc}][C_2]^{-1}$ of the above equation can be determined by substituting the values of $[C_2]$, $[r_{abc}]$ and $[C_2]^{-1}$ as:

$$\begin{aligned} [C_2][r_{abc}][C_2]^{-1} &= \\ i \begin{bmatrix} \cos\theta_r & \cos(\theta_r - \frac{2\pi}{3}) & \cos(\theta_r + \frac{2\pi}{3}) \\ \sin\theta_r & \sin(\theta_r - \frac{2\pi}{3}) & \sin(\theta_r + \frac{2\pi}{3}) \\ \frac{1}{2} & \frac{1}{2} & \frac{1}{2} \end{bmatrix} \begin{bmatrix} r_a & 0 & 0 \\ 0 & r_b & 0 \\ 0 & 0 & r_c \end{bmatrix} \begin{bmatrix} \cos\theta_r & \sin\theta_r & 1 \\ \cos(\theta_r - \frac{2\pi}{3}) & \sin(\theta_r - \frac{2\pi}{3}) & 1 \\ \cos(\theta_r + \frac{2\pi}{3}) & \sin(\theta_r + \frac{2\pi}{3}) & 1 \end{bmatrix} \end{aligned} \quad (3.91)$$

The evaluation of the above matrices yields

$$[C_2]\{[r_{abc}][C_2]^{-1} = [r_{abc}] \quad (3.92)$$

The second term of equation (3.90) can be evaluated as

$$[C_2]p[C_2]^{-1}[\lambda_{qbm}^r] = \omega_r \begin{bmatrix} 0 & 1 & 0 \\ -1 & 0 & 0 \\ 0 & 0 & 0 \end{bmatrix} \begin{bmatrix} \lambda_q \\ \lambda_d \\ \lambda_0 \end{bmatrix} = \omega_r \begin{bmatrix} \lambda_d \\ \lambda_q \\ 0 \end{bmatrix} \quad (3.93)$$

Equation (3.93) can be also be written as

$$[\ell'_{-2}]p[\ell'_{-2}]^{-1}[\lambda'_{t\phi}] = \omega_r \lambda'_{t\phi} \quad (3.94)$$

and since

$$[\ell'_{-2}][\ell'_{-2}]^{-1} = 1$$

The last term of equation (3.90) becomes

$$[\ell'_{-2}][\ell'_{-2}]^{-1}p[\lambda'_{r\phi}] = p[\lambda'_{r\phi}] \quad (3.95)$$

Now the voltage equation (3.90) can be written with the values given in equations (3.92)-(3.95) as:

$$[v'_{r\phi}] = [r_{r\phi}][i'_{r\phi}] + \omega_r[\lambda'_{t\phi}] + p[\lambda'_{r\phi}] \quad (3.96)$$

or

$$\begin{bmatrix} v'_r \\ v'_d \\ v'_0 \end{bmatrix} = \begin{bmatrix} r_a & 0 & 0 \\ 0 & r_b & 0 \\ 0 & 0 & r_c \end{bmatrix} \begin{bmatrix} i'_r \\ i'_d \\ i'_0 \end{bmatrix} + \omega_r \begin{bmatrix} \lambda'_d \\ \lambda'_q \\ 0 \end{bmatrix} + p \begin{bmatrix} \lambda'_r \\ \lambda'_q \\ \lambda'_0 \end{bmatrix} \quad (3.97)$$

If it is assumed that stator resistance in each phase is equal, i.e.

$$r_a = r_b = r_c = r_s \quad (3.98)$$

then from equation (3.97) it can be written that

$$v'_r = r_s i'_r + \omega_r \lambda'_d + p \lambda'_r \quad (3.99)$$

$$v'_d = r_s i'_d + \omega_r \lambda'_q + p \lambda'_d \quad (3.100)$$

$$v'_0 = r_s i'_0 + p \lambda'_0 \quad (3.101)$$

Now, λ'_t, λ'_g and λ'_0 can be determined in the following way:

From equation (3.70), it can be written that

$$[\lambda_{ab}] = [L][i_{ab}] + [\lambda_F] \quad (3.102)$$

If it is transformed to the rotor reference frame, then it becomes

$$[\lambda'_{rt}] = [C_2][\lambda_{ab}] \quad (3.103)$$

Now substituting equation (3.102) in (3.103) yields

$$\begin{aligned} [\lambda'_{rt}] &= [C_2][L][i_{ab}] + [C_2][\lambda_F] \\ &= [C_2][L][C_2]^{-1}[i'_{tab}] + [C_2][\lambda_F] \end{aligned} \quad (3.104)$$

The first term of equation (3.104) is evaluated by putting the values of $[C_2]$, $[L]$ and $[C_2]^{-1}$ from the equations (3.82), (3.56) and (3.84), respectively and after some trigonometric manipulations, the following equation is obtained,

$$[C_2][L][C_2]^{-1}[i'_{tab}] = \begin{bmatrix} L_t + \frac{3}{2}(L_A - L_B) & 0 & 0 \\ 0 & L_t + \frac{3}{2}(L_A + L_B) & 0 \\ 0 & 0 & L_t \end{bmatrix} \begin{bmatrix} i'_t \\ i'_d \\ i'_0 \end{bmatrix} \quad (3.105)$$

The second term of equation (3.104) can be evaluated by putting the values of $[C_2]$ and $[\lambda_F]$ from equations (3.82) and (3.65) respectively. Again, after some trigonometric manipulations, one gets

$$[C_2][\lambda_F] = \frac{2}{3}\lambda_M \begin{bmatrix} 0 \\ \frac{\sqrt{3}}{2} \\ 0 \end{bmatrix} = \lambda_M \begin{bmatrix} 0 \\ 1 \\ 0 \end{bmatrix} \quad (3.106)$$

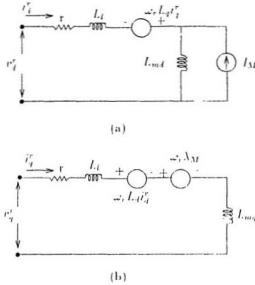


Figure 3.3: Park's model of permanent magnet synchronous motor: (a) d axis (b) q-axis

Now defining the magnetizing inductances in equation (3.105) as

$$\frac{3}{2}(L_A - L_B) = L_{mq} \quad (3.107)$$

$$\frac{3}{2}(L_A + L_B) = L_{md} \quad (3.108)$$

and letting $L_q = L_l + L_{mq}$ and $L_d = L_l + L_{md}$, it can be written that

$$\begin{bmatrix} \lambda_q' \\ \lambda_d' \\ \lambda_0' \end{bmatrix} = \begin{bmatrix} L_q & 0 & 0 \\ 0 & L_d & 0 \\ 0 & 0 & L_l \end{bmatrix} \begin{bmatrix} i_q' \\ i_d' \\ i_0' \end{bmatrix} + \lambda_M \begin{bmatrix} 0 \\ 1 \\ 0 \end{bmatrix} \quad (3.109)$$

Therefore,

$$\lambda_q' = L_q i_q' \quad (3.110)$$

$$\lambda'_d = L_d i'_d + \lambda_M \quad (3.111)$$

$$\lambda'_q = L_q i'_q \quad (3.112)$$

Now substituting equations (3.110) and (3.111) in (3.99) and (3.100) respectively, and ignoring the zero sequence terms, one gets

$$v'_q = (r_s + pL_q)i'_q + \omega_r L_d i'_d + \omega_r \lambda_M \quad (3.113)$$

$$v'_d = (r_s + pL_d)i'_d - \omega_r L_q i'_q \quad (3.114)$$

Using equations (3.113) and (3.114) the permanent magnet synchronous motor can be represented in d and q axes with the equivalent circuit diagram as shown in Fig. 3.3.

The next step is to establish a relationship between orthogonal quantities of rotating and stationary reference frames.

3.3.3 Relationship between orthogonal quantities of stationary reference frame and synchronously rotating reference frame

Relationship can be established between quadrature and direct axes variables of the stationary reference frame and the rotating reference frame by the following equation:

$$[x'_{r0}] = [C'_{\alpha}] [x'_{s0}] \quad (3.115)$$

where superscripts 'r' and 's' are used to denote rotating and stationary reference frame quantities, respectively. $[C'_{\alpha}]$ is the coefficient matrix which can be evaluated as follows:

From equation (3.76), it can be written that

$$[x'_{r0}] = [C'_{\alpha}] [x_{s0}] \quad (3.116)$$

Substituting equation (3.116) into (3.115), one gets

$$[x'_{i0}] = [\ell'_{31}][\ell'_{1i}][x_{ib}] \quad (3.117)$$

Again following the relation of equation (3.85), it can be written as

$$[x'_{i0}] = [\ell'_{2i}][x_{ib}] \quad (3.118)$$

Thus comparing equation (3.117) and (3.118), it can be written that

$$[\ell'_{3i}][\ell'_{1i}][x_{ib}] = [\ell'_{2i}][x_{ib}] \quad (3.119)$$

from which

$$[\ell'_{3i}] = [\ell'_{2i}][\ell'_{1i}]^{-1} \quad (3.120)$$

Now substituting the value of $[\ell'_{2i}]$ and $[\ell'_{1i}]^{-1}$ from equations (3.82) and (3.81) in (3.120) one gets,

$$[\ell'_{3i}] = \begin{bmatrix} \cos(\theta_r) & -\sin(\theta_r) & 0 \\ \sin(\theta_r) & \cos(\theta_r) & 0 \\ 0 & 0 & 1 \end{bmatrix} \quad (3.121)$$

From equation (3.115) it can be written that

$$[x'_{i0}] = [\ell'_{3i}]^{-1}[x'_{i0}] \quad (3.122)$$

and

$$[\ell'_{3i}]^{-1} = [\ell'_{3i}]^T \quad (3.123)$$

Now substituting r for x in equation (3.115), one gets

$$[r'_{i0}] = [\ell'_{3i}][r'_{i0}] \quad (3.124)$$

substituting the value of $[C_3]$ from equation (3.121) and expanding yields,

$$v_q^r = v_q^s \cos \theta_r - v_d^s \sin \theta_r \quad (3.125)$$

$$v_d^r = -v_q^s \sin \theta_r + v_d^s \cos \theta_r \quad (3.126)$$

where zero sequence terms are ignored. Similarly, using equations (3.122) and (3.123) it can be written that

$$[v_{\tau\theta}^s] = [C_3]^{-1} [v_{\tau\theta}^r] \quad (3.127)$$

Again ignoring zero sequence terms and expanding, one gets

$$v_q^s = v_q^r \cos \theta_r + v_d^r \sin \theta_r \quad (3.128)$$

$$v_d^s = -v_q^r \sin \theta_r + v_d^r \cos \theta_r \quad (3.129)$$

The same relationships can be established for currents as given below:

$$i_q^r = i_q^s \cos \theta_r - i_d^s \sin \theta_r \quad (3.130)$$

$$i_d^r = i_q^s \sin \theta_r + i_d^s \cos \theta_r \quad (3.131)$$

$$i_q^s = i_q^r \cos \theta_r + i_d^r \sin \theta_r \quad (3.132)$$

$$i_d^s = i_d^r \cos \theta_r - i_q^r \sin \theta_r \quad (3.133)$$

where θ_r as defined previously is

$$\theta_r = \int_0^t \omega_r(t) dt + \theta_r(0) \quad (3.134)$$

and $\omega_r(t)$ is the synchronous speed of rotating frame, $\theta_r(0)$ is the time-zero displacement of rotating frame quadrature axis with respect to quadrature axis of stationary frame, i.e. a axis of three phase voltages as shown in Fig. 3-4.

The next step is to establish a relation between direct and quadrature axes quantities and three phase quantities, so that the algorithm can be used to obtain rotor position and speed information with measured stator voltages and currents.

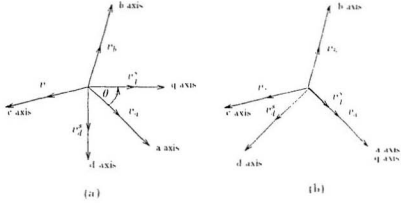


Figure 3.1: (a) Co-ordinate systems of the stationary reference frame with an initial θ . (b) Co-ordinate systems of stationary reference frame with $\theta = 0$.

3.3.4 Relationship between three-phase and orthogonal quantities in stationary reference frame

In this section, three-phase machine equations are transformed into direct and quadrature axis on the same stationary reference frame. So equations (3.76) (3.79) can be used for this analysis. Here the value of θ in equation (3.80) is evaluated as follows:

$$\theta = \int_0^t \omega(t) dt + \theta(0) \quad (3.135)$$

It has been already mentioned that ω is the speed of the transformed frame, and for this particular case as transformation is considered from stationary to stationary, $\omega = 0$. It is also assumed that $\theta(0)$ is zero by considering the 'a' axis to coincide with q axis as shown in the Fig. 3.1. Superscript s will be used to denote that transformation is taking place between stationary to stationary frame. Substituting

$\theta = 0$, $[C_4]$ of equation (3.79) now becomes

$$[C_4] = \frac{k}{3} \begin{bmatrix} 1 & -\frac{1}{2} & -\frac{1}{2} \\ 0 & -\frac{\sqrt{3}}{2} & \frac{\sqrt{3}}{2} \\ \frac{1}{2} & \frac{1}{2} & \frac{1}{2} \end{bmatrix} \quad (3.136)$$

and the inverse of $[C_4]$ becomes

$$[C_4]^{-1} = \begin{bmatrix} 1 & 0 & 1 \\ -\frac{1}{2} & -\frac{\sqrt{3}}{2} & 1 \\ -\frac{1}{2} & \frac{\sqrt{3}}{2} & 1 \end{bmatrix} \quad (3.137)$$

so the quadrature and direct axes voltages can be found as:

$$[v_{qm}] = [C_4][v_{abc}] \quad (3.138)$$

from which

$$[v_{abc}] = [C_4]^{-1}[v_{qm}] \quad (3.139)$$

Substituting equations (3.136) and (3.137) in equations (3.138) and (3.139) and expanding one gets

$$\begin{aligned} v_q^s &= \frac{2}{3}(v_a - \frac{1}{2}v_b - \frac{1}{2}v_c) \\ &= \frac{2}{3}v_a - \frac{1}{3}v_b - \frac{1}{3}v_c \end{aligned} \quad (3.140)$$

but since $v_a + v_b + v_c = 0$, it can be written that

$$\frac{1}{3}v_a = -\frac{1}{3}v_b - \frac{1}{3}v_c \quad (3.141)$$

Substituting equation (3.141) in equation (3.140) one obtains

$$v_q^s = \frac{2}{3}v_a + \frac{1}{3}v_a = v_a \quad (3.142)$$

and

$$\begin{aligned} v_d^* &= \frac{2}{3} \left(-\frac{\sqrt{3}}{2} v_b + \frac{\sqrt{3}}{2} v_c \right) \\ &= -\frac{1}{\sqrt{3}} v_b + \frac{1}{\sqrt{3}} v_c. \end{aligned} \quad (3.143)$$

Inversely,

$$v_b = v_d^* \quad (3.144)$$

$$v_b = -\frac{1}{2} v_d^* - \frac{\sqrt{3}}{2} v_d^* \quad (3.145)$$

$$v_c = -\frac{1}{2} v_d^* + \frac{\sqrt{3}}{2} v_d^* \quad (3.146)$$

Proceeding in the same manner, the same relationship can be established among the three-phase currents and direct and quadrature axes currents in the same stationary frame which is given as:

$$i_d^* = i_a \quad (3.147)$$

$$i_d^* = -\frac{1}{\sqrt{3}} i_b + \frac{1}{\sqrt{3}} i_c \quad (3.148)$$

Inversely

$$i_a = i_d^* \quad (3.149)$$

$$i_b = -\frac{1}{2} i_d^* - \frac{\sqrt{3}}{2} i_d^* \quad (3.150)$$

$$i_c = -\frac{1}{2} i_d^* + \frac{\sqrt{3}}{2} i_d^* \quad (3.151)$$

3.4 Rotor-speed and rotor-position in terms of stator currents and voltage

The direct axis voltage equation of Park's machine model derived in the earlier section is given as

$$v_d^s = (r_s + pL_d)i_d^s - \omega_r L_q i_q^s \quad (3.152)$$

Substituting equations (3.130) and (3.131) in equation (3.152) one gets

$$\begin{aligned} v_d^s &= (r_s + pL_d)(i_q^s \sin \theta_r + i_d^s \cos \theta_r) + \\ &\quad \omega_r L_q (i_q^s \cos \theta_r - i_d^s \sin \theta_r) \\ &= \cos \theta_r [r_s i_d^s + L_d p i_d^s - \omega_r (L_q - L_d) i_q^s] + \\ &\quad \sin \theta_r [r_s i_q^s + L_d p i_q^s + \omega_r (L_q - L_d) i_d^s] \end{aligned} \quad (3.153)$$

Now putting equation (3.126) in (3.153) one gets

$$\begin{aligned} v_d^s \sin \theta_r + v_q^s \cos \theta_r &= \cos \theta_r [r_s i_d^s + L_d p i_d^s - \omega_r (L_q - L_d) i_q^s] + \\ &\quad \sin \theta_r [r_s i_q^s + L_d p i_q^s + \omega_r (L_q - L_d) i_d^s] \end{aligned} \quad (3.154)$$

Or,

$$\begin{aligned} \cos \theta_r [r_s i_d^s + L_d p i_d^s - \omega_r (L_q - L_d) i_q^s] &= \\ \sin \theta_r [v_d^s - r_s i_q^s - L_d p i_q^s - \omega_r (L_q - L_d) i_d^s] \end{aligned} \quad (3.155)$$

Therefore

$$\tan \theta_r = \frac{-v_d^s + r_s i_q^s + L_d p i_q^s - \omega_r (L_q - L_d) i_d^s}{v_d^s - r_s i_q^s - L_d p i_q^s - \omega_r (L_q - L_d) i_d^s} \quad (3.156)$$

Or

$$\theta_r = \tan^{-1} \left[\frac{-v_d^s + r_s i_q^s + L_d p i_q^s - \omega_r (L_q - L_d) i_d^s}{v_d^s - r_s i_q^s - L_d p i_q^s - \omega_r (L_q - L_d) i_d^s} \right] \quad (3.157)$$

The position of rotor can thus be obtained in terms of machine voltages and currents in the stator frame provided ω_r in equation (3.157) can be evaluated in terms of voltages and currents. For this purpose, Park's quadrature axis voltage equation (3.113) is used. From this equation it can be written that

$$v_q^r = (r_s + pL_q)i_q^r + \omega_r L_q i_d^r + \omega_r \lambda_M \quad (3.158)$$

Substituting equations (3.130) and (3.131) in (3.158), the following equations are obtained:

$$\begin{aligned} v_q^r &= (r_s + pL_q)(i_q^s \cos \theta_r - i_d^s \sin \theta_r) + \\ &\quad \omega_r L_q (i_q^s \sin \theta_r + i_d^s \cos \theta_r) + \omega_r \lambda_M \\ &= \cos \theta_r [r_s i_q^s + L_q p i_q^s - \omega_r (L_q - L_d) i_d^s] + \\ &\quad \sin \theta_r [-r_s i_d^s - L_q p i_d^s - \omega_r (L_q - L_d) i_q^s] + \omega_r \lambda_M \end{aligned} \quad (3.159)$$

Substituting equation (3.125) in (3.159), one obtains

$$\begin{aligned} v_q^s \cos \theta_r - v_d^s \sin \theta_r &= \cos \theta_r [r_s i_q^s + L_q p i_q^s - \omega_r (L_q - L_d) i_d^s] + \\ &\quad \sin \theta_r [-r_s i_d^s - L_q p i_d^s - \omega_r (L_q - L_d) i_q^s] + \omega_r \lambda_M \end{aligned} \quad (3.160)$$

Substituting equations (3.142), (3.143), (3.147) and (3.148) in equation (3.160) one obtains

$$\begin{aligned} \cos \theta_r [v_k - r_s i_k - L_q p i_k - \frac{1}{\sqrt{3}} \omega_r (L_q - L_d) (i_b - i_c)] &= \\ \sin \theta_r [-\frac{1}{\sqrt{3}} (v_b - v_c) + \frac{1}{\sqrt{3}} r_s (i_b - i_c) + \\ \frac{1}{\sqrt{3}} L_q p (i_b - i_c) + \frac{1}{\sqrt{3}} \omega_r (L_q - L_d) (i_b - i_c)] + \omega_r \lambda_M \end{aligned} \quad (3.161)$$

Or,

$$\begin{aligned} \frac{\omega_r \lambda_M}{\cos \theta_r} = & \\ & v_a - r_s i_a - L_q p i_a - \frac{1}{\sqrt{3}} \omega_r (L_q - L_d)(i_b - i_c) \\ & - \tan \theta_r \left[-\frac{1}{\sqrt{3}}(v_b - v_c) + \frac{1}{\sqrt{3}} r_s (i_b - i_c) + \frac{1}{\sqrt{3}} L_q p (i_b - i_c) + \right. \\ & \left. \frac{1}{\sqrt{3}} \omega_r (L_q - L_d)(i_b - i_c) \right] \end{aligned} \quad (3.162)$$

Substituting equations (3.142), (3.143), (3.147) and (3.148) in equation (3.155) and assuming

$$x = v_a - r_s i_a - L_d p i_a + \frac{1}{\sqrt{3}} \omega_r (L_q - L_d)(i_b - i_c) \quad (3.163)$$

$$y = \frac{1}{\sqrt{3}}(v_b - v_c) - \frac{1}{\sqrt{3}} r_s (i_b - i_c) - \frac{1}{\sqrt{3}} L_d p (i_b - i_c) - \omega_r (L_q - L_d) i_a \quad (3.164)$$

one obtains

$$\tan \theta_r = \frac{y}{x} \quad (3.165)$$

$$\cos \theta_r = \frac{x}{z} \quad (3.166)$$

where

$$z = \sqrt{x^2 + y^2} \quad (3.167)$$

The expression for ω_r can be simplified by taking equal value for L_q and L_d which can be assumed as [31]

$$L_s = \frac{(L_q + L_d)}{2} \quad (3.168)$$

Now substituting (3.168) in equations (3.162)-(3.161) yields

$$\begin{aligned} \frac{\omega_r \lambda_M}{\cos \theta_r} = & \\ & v_a - r_s \dot{i}_a - L_s p \dot{a} - \tan \theta_r \left\{ -\frac{1}{\sqrt{3}}(v_b - v_c) + \frac{1}{\sqrt{3}} r_s (\dot{i}_b - \dot{i}_c) \right\} \\ & + \frac{1}{\sqrt{3}} L_s p (\dot{i}_b - \dot{i}_c) \end{aligned} \quad (3.169)$$

$$x = v_a - r_s \dot{i}_a - L_s p \dot{a} \quad (3.170)$$

$$y = \frac{1}{\sqrt{3}} [v_b - v_c - r_s (\dot{i}_b - \dot{i}_c) - L_s p (\dot{i}_b - \dot{i}_c)] \quad (3.171)$$

Therefore from equation (3.157), it can be written that

$$\tan \theta_r = \frac{y}{x} = \frac{\frac{1}{\sqrt{3}} [v_b - v_c - r_s (\dot{i}_b - \dot{i}_c) - L_s p (\dot{i}_b - \dot{i}_c)]}{v_a - r_s \dot{i}_a - L_s p \dot{a}} \quad (3.172)$$

$$\begin{aligned} \cos \theta_r = \frac{x}{\sqrt{(x^2 + y^2)}} = & \\ & \frac{v_a - r_s \dot{i}_a - L_s p \dot{a}}{\sqrt{[(v_a - r_s \dot{i}_a - L_s p \dot{a})^2 + \left\{ \frac{1}{\sqrt{3}} \{v_b - v_c - r_s (\dot{i}_b - \dot{i}_c) - L_s p (\dot{i}_b - \dot{i}_c)\} \right\}^2]}} \end{aligned} \quad (3.173)$$

Substituting equations (3.172) and (3.173) in equation (3.169) and simplifying one gets

$$\omega_r = \frac{\sqrt{(v_a - r_s \dot{i}_a - L_s p \dot{a})^2 + \left\{ \frac{1}{\sqrt{3}} [v_b - v_c - r_s (\dot{i}_b - \dot{i}_c) - L_s p (\dot{i}_b - \dot{i}_c)] \right\}^2}}{\lambda_M} \quad (3.174)$$

The rotor position θ_r can be found by substituting the value of ω_r in the following equation:

$$\theta_r = \tan^{-1} \left[\frac{v_b - v_c - r_s (\dot{i}_b - \dot{i}_c) - L_s p (\dot{i}_b - \dot{i}_c) - \sqrt{3} \omega_r (L_q - L_d) \dot{a}}{\sqrt{3} (v_a - r_s \dot{i}_a - L_d p \dot{a}) + \omega_r (L_q - L_d) (\dot{i}_b - \dot{i}_c)} \right] \quad (3.175)$$

Thus from equation (3.174) and (3.175), one obtains

$$\theta_r = \tan^{-1} \left[\frac{A}{B} \right] \quad (3.176)$$

where

$$A = \lambda_M \{v_b - v_r - r_s(i_b - i_r) - L_d p(i_b - i_r)\} - (L_q - L_d)i_a \\ \times \sqrt{3(v_a - r_s i_a - L_d p i_a)^2 + \{v_b - v_r - r_s(i_b - i_r) - L_d p(i_b - i_r)\}^2}$$

and

$$B = \sqrt{3} \lambda_M (v_a - r_s i_a - L_d p i_a) + (L_q - L_d)(i_b - i_r) \\ \times \sqrt{(v_a - r_s i_a - L_d p i_a)^2 + \frac{1}{3} \{v_b - v_r - r_s(i_b - i_r) - L_d p(i_b - i_r)\}^2}$$

The initial position angle θ_{r0} or time-zero position of rotor can be determined by putting $\omega_r = 0$ in equation (3.175) which follows;

$$\theta_{r0} = \tan^{-1} \left[\frac{\frac{1}{\sqrt{3}} \{v_b - v_r - r_s(i_b - i_r) - L_d p(i_b - i_r)\}}{v_a - r_s i_a - L_d p i_a} \right] \quad (3.177)$$

3.5 Summary

In this chapter, expressions for the rotor speed and rotor position in terms of stator voltages and currents of the permanent magnet synchronous motor have been derived. In the next chapter, these expressions are used to simulate the vector control scheme of the permanent magnet synchronous motor.

Chapter 4

Simulation of position sensorless permanent magnet synchronous motor drive

The present work deals with rotor position estimation for the vector control of permanent magnet synchronous motor drives. In chapter three, expressions of rotor speed and rotor position were derived in terms of stator voltages and currents for computational purposes. In this chapter, computer simulation of drive systems are provided for the following configurations:

1. PMS motor with sinusoidal supply without control scheme.
2. PMS motor drive system with only speed loop up to base speed [31].
3. PMS drive system with speed and torque loops operated up to the base speed.
4. PMS drive system with speed and torque loops at any speed (ω below or above the base speed).

Each configuration is provided with its block diagram, flow chart and simulation results.

4.1 Simulation of permanent magnet synchronous motor with sinusoidal supply without control scheme.

The system block diagram is shown in Fig. 4.1 for this simulation.

A set of 3 phase balanced ac supply can be written as

$$v_a = V_m \cos \omega t \quad (4.1)$$

$$v_b = V_m \cos \left(\omega t - \frac{2\pi}{3} \right) \quad (4.2)$$

$$v_c = V_m \cos \left(\omega t + \frac{2\pi}{3} \right) \quad (4.3)$$

These balanced 3 phase voltages are applied to the stator terminals of the permanent magnet synchronous motor. The resulting phase currents are given by

$$i_a = I_m \cos(\omega t - \gamma) \quad (4.4)$$

$$i_b = I_m \cos \left(\omega t - \frac{2\pi}{3} - \gamma \right) \quad (4.5)$$

$$i_c = I_m \cos \left(\omega t + \frac{2\pi}{3} - \gamma \right) \quad (4.6)$$

where γ is the phase angle between phase voltage and current. These input voltages and currents are measured and transformed to direct and quadrature axes in stator frame. These are used for the sensorless algorithm derived in equations (3.174) and (3.176). The sensorless algorithm can be implemented by a fast digital signal processor such as the Texas Instrument TMS320C4X. The inputs to the digital processor are

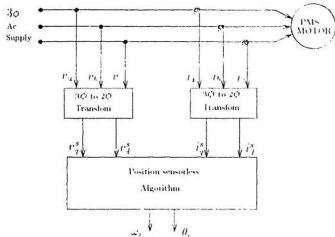


Figure 4.1: Block diagram of open loop simulation of PMS motor

phase voltages and phase currents transformed to d-q quantities. The outputs are rotor speed ω_r and rotor position $\text{ang}_r = \theta_r$. Fig. 4.2 contains the flow chart for open loop simulation of PMS motor with sinusoidal supply voltage. Fig. 4.3 (a) shows the simulated speed as a function of time for the open loop control of the PMS motor. Fig. 4.3 (b) shows the simulated rotor position angle as a function of time for open loop control case.

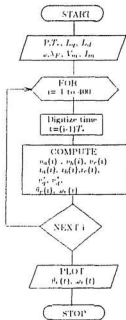


Figure 4.2: Flow chart for open loop simulation of PMS motor

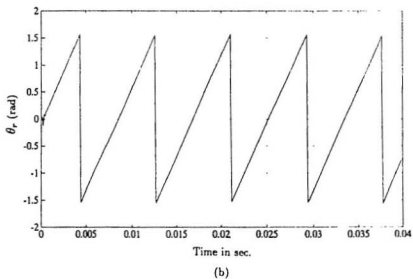
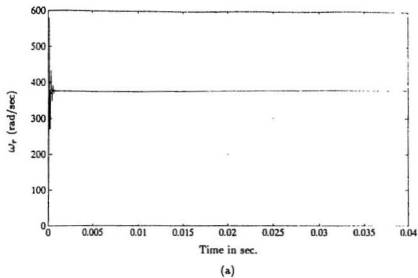


Figure 4.3: Open loop simulation of PMS motor. (a) Rotor speed. (b) Rotor position angle.

4.2 Simulation of closed loop vector control of permanent magnet synchronous motor

As mentioned earlier, the PMS motor can be controlled vectorically when the stator variables are transformed to the synchronously rotating reference frame axis where the sinusoidal quantities appear as dc quantities. So from the concept of dc motor control, the developed torque T_e can be expressed as

$$T_e = K_t I_a I_f \quad (4.7)$$

where I_a is the armature current and I_f is the field current; and both are orthogonal and decoupled vectors. In synchronously rotating rotor frame axis, torque equation (4.7) can be written as

$$T_e = K_t i_q^r I_f \quad (4.8)$$

where i_q^r is the quadrature axis current component in rotor reference frame corresponding to torque; and I_f is the equivalent field current produced by the rotor permanent magnet. Since in permanent magnet synchronous machine, synchronously rotating rotor produces constant flux of λ_M , the torque equation (4.8) can be expressed as

$$T_e = K_m i_q^r \lambda_M \quad (4.9)$$

Thus the motor can be controlled vectorically provided the current i_q^r is controlled. In practice, the speed of a PMS motor can be controlled precisely if i_q^r can be obtained at desired speeds by using various types of controllers such as proportional (P), proportional integral (PI) or proportional integral differential (PID) controllers. The current i_q^r can be used to drive an inverter to operate a motor at different speeds. Before going into further details of control aspects, the relation between the peak

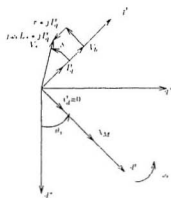


Fig. (a)

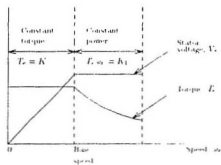


Fig. (b)

Figure 4.4: (a) Vector diagram for drives upto base speed [41]. (b) Torque speed characteristics.

value of the applied voltage and the I_q^* is established first with the help of the vector diagram. In the vector diagram of Fig. 4.4(a), λ_M is shown on the direct axis of the rotating frame. Hence, the back emf produced will be on the quadrature axis and is given by

$$V_b = \frac{j\omega_r \lambda_M}{c_1} \quad (4.10)$$

where c_1 is a constant, the value of which is given by 1.5 [41]. Thus from vector diagram of Fig. 4.4(a), the applied voltage is given by

$$V_s = V_b + (r + j\omega_r L_s)jI_q^* \quad (4.11)$$

So the three phase voltages and currents are now known quantities corresponding to a desired speed of the motor. These known quantities are used in the simulation of the drive system.

4.2.1 PMS motor drive system upto base speed with speed feedback loop only

This system is capable of operating upto base speed only [31]. The torque is maintained constant upto the base speed as shown in Fig. 4.4(b). Thus, for this drive, constant voltage to frequency ratio is maintained which is obtained from the PWM operation of the voltage source inverter (VSI). The feedback loop used is only the speed. The whole drive system can be described by the following block diagram as shown in Fig. 4.5.

The block diagram (Fig. 4.5) consists of a number of small blocks which are designed to perform specific functions for the operation of the drive. The general descriptions and the functions of these blocks are discussed below:

PI controller

The proportional integral (PI) controller consists of the following transfer function in the Laplace domain as

$$G(s) = K_1 + \frac{K_2}{s} \quad (4.12)$$

where K_1 corresponds to the proportional part and $\frac{K_2}{s}$ accounts for the integral part. If the input of PI controller is $X(s)$ and the output is $Y(s)$, then it can be written that

$$\frac{Y(s)}{X(s)} = K_1 + \frac{K_2}{s} \quad (4.13)$$

which can also be written in the form

$$sY(s) = K_2X(s) + K_1sX(s) \quad (4.14)$$

If T_s is taken as the sampling period and is considered very small, then the derivative can be written in finite difference form as

$$\frac{Y(n+1) - Y(ii)}{T_s} = K_2X(ii) + K_1 \left[\frac{X(ii+1) - X(ii)}{T_s} \right] \quad (4.15)$$

where $ii, n+1$ are the subsequent sampling instants. Now equation (4.15) can be written as

$$Y(ii+1) = Y(ii) + K_2T_sX(ii) + K_1X(ii+1) - K_1X(ii) \quad (4.16)$$

The equation (4.16) is used to simulate the PI controller blocks.

The function of the PI controller used in the block diagram (Fig. 4.5) is to give a current command from the error signal of command speed and actual speed.

Vector rotator

This is the block which transfers the rotor reference frame quantities to stator reference frame quantities. By this block, the command output i_t^{**} and i_d^{**} are formulated using equations (3.130) and (3.131) with command input currents i_t^* , i_d^* and unit vectors $\cos \theta_r$, $\sin \theta_r$.

2 phase-3 phase transfer block

The function of this block is to transfer the d-q stator currents to the three phase stator currents. The three phase stator currents are used as references of the current controller as shown in Fig. 4.6.

4.2.2 Current controller and voltage source inverter (VSI)

The schematic diagram of the current controller and the voltage source inverter is shown in Fig. 4.6. The current controllers proposed for this drive are known as the hysteresis current controllers. The functional block diagram of this current controller is shown in Fig. 4.7. In these current controllers, the output of the 2 phase-3 phase transfer block, the sine reference waveforms are compared with the actual phase currents. The actual phase currents are allowed to vary within a prescribed higher and lower limit known as the hysteresis band. When the actual phase current exceeds the higher limit (Fig. 4.7 (b)), the upper transistor of the half bridge for that particular phase is turned off and the lower one is turned on, giving a change of output voltage from the positive half of inverter dc voltage to the negative half. When this switching action occurs, the phase currents start decaying, as shown in Fig. 4.7 (b). As the phase currents just reach the lower limit of the hysteresis band, the lower transistor is turned off and the upper one is again turned on. In this particular fashion, the

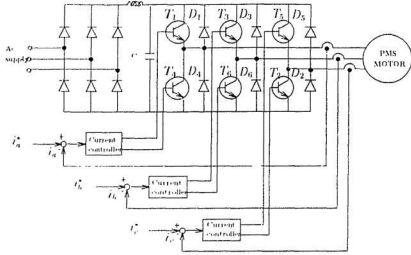
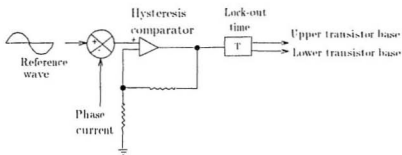


Figure 1.6: Voltage source inverter and current controller [39]

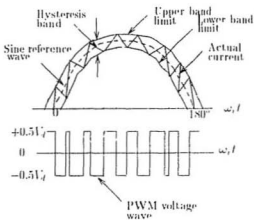
switching action of the inverter, goes on and the actual current wave is forced to track the reference wave within the hysteresis band'. Because of the use of this type of current controller, the phase currents are considered as sinusoidal.

Initial rotor position estimator block

For the implementation of the proposed drive scheme, the initial position of the rotor needs to be obtained. This is done by feeding a high frequency triangular wave to the vector rotator before the INTERRUPT switches actuate [31]. By the application of such a signal, the rotor does not move due to the zero average torque. Initially, the arbitrary unit vectors $\cos \theta_r = 1, \sin \theta_r = 0$ are applied to the vector rotator to get the reference signal for the current controller which drives the inverter. The output



(a)



(b)

Figure 1.7: (a) Hysteresis current controller (b) Inverter output [39]

of the inverter is the PWM voltage which is applied to the machine. This results in small pulsating motion of the rotor. By measuring phase currents and voltages, the initial rotor position θ_0 can be estimated using equation (3.177).

Polarity detection block

The actual initial position of the rotor is dependent on the polarity of the magnet which is in the vicinity of a reference axis of the stator. For example, if N pole is in the vicinity of phase a , then the true initial position will be

$$\theta_m = 0 + \theta_0$$

but if S pole is close to phase a , then

$$\theta_m = \pi + \theta_0$$

The polarity of the magnet can be determined by the following procedure [31]. A square wave is applied to phase a . If N pole is in the vicinity of a axis, then the positive part of the applied voltage will aid in the magnetization and negative part will decrease the magnetization. Hence the phase current with this voltage will be greater for the positive part than that due to the negative part of the square wave. If the reverse be the case, then it can be concluded that S pole is close to a axis. Thus, by following the above procedure, decision is taken as to which one is added to θ_0 , 0 or π .

Rotor position and speed estimator

Using equations (3.174) and (3.176), this block outputs the speed ω_r and the rotor position θ_r . Once θ_r is known, the unit vectors $\sin \theta_r$ and $\cos \theta_r$ are generated. This block starts working after the actuation of INTERRUPT switch.

4.2.3 Working principle of the drive system

The command speed ω_r^* is applied to the PI controller which outputs the reference current i_q^* . With the initial unit vector $\sin \theta_{r0}$ and $\cos \theta_{r0}$, the vector rotator produces the quadrature and direct axes reference currents which are transformed to three-phase sine reference currents for the input of the hysteresis current controller. The current controller drives the inverter giving PWM voltages to the machine terminal. As the motor is started, the interrupt switches are turned on and the estimator estimates the rotor speed and rotor position and the unit vectors. Next the estimated rotor speed is fed back to the command speed for comparison and the estimated unit vectors are fed to the vector rotator to generate command stator currents.

This drive system is operated up to base speed. Thus the command speed is given up to that limit. The flow chart of the computer simulation of the PMS motor drive with PI controllers is given in Fig. 4.8 The simulation has been carried out with the sampling frequency taken at 10000 Hz. The constants of the PI controller have been taken as $K_1 = 0.001$ and $K_2 = 6$.

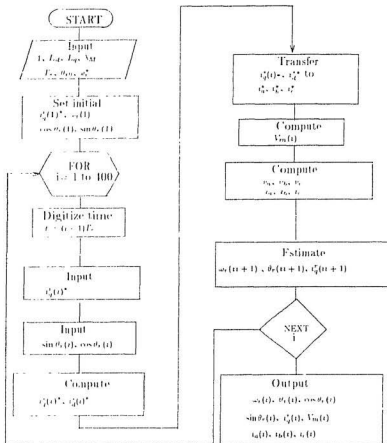


Figure 4.8: Flow chart of PMS motor drive with one feed back speed loop (upto base speed).

Fig. 4.9-4.12 show the simulated reference speed, actual rotor speed, rotor position, unit vectors, phase currents, reference torque component current and output voltage of the inverter with speed feed back control.

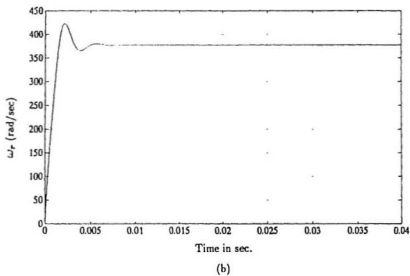
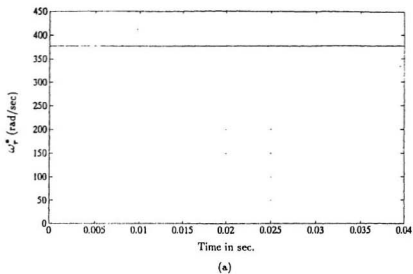


Figure 4.9: Simulation of single loop (speed loop) PMS motor drive. (a) Reference rotor speed. (b) Actual rotor speed.

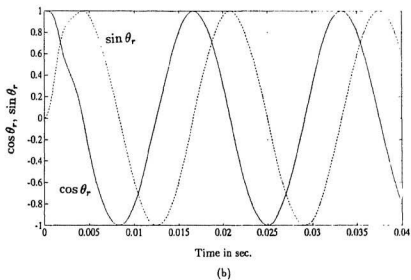
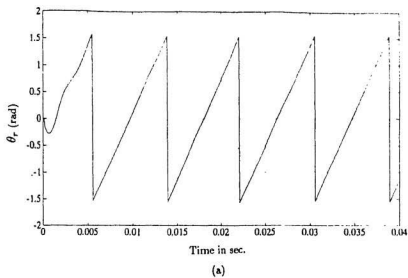


Figure 4.10: Simulation of single loop (speed loop) PMS motor drive. (a) Rotor position (b) Unit vectors.

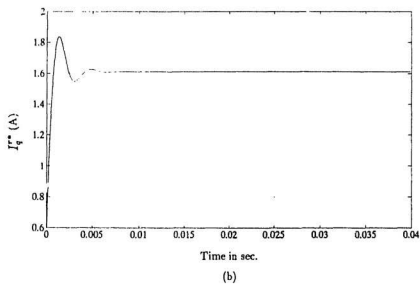
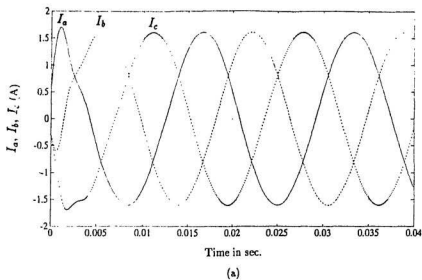


Figure 1.11: Simulation of single loop (speed loop) PMS motor drive. (a) Phase currents (b) Reference torque component current

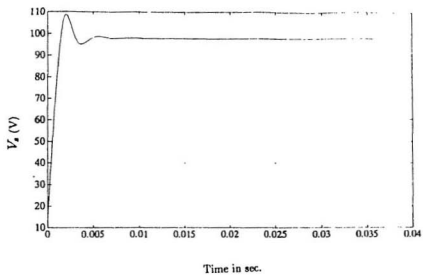


Figure 4.12: Output voltage of the inverter

4.3 PMS motor drive with two control loops

The permanent magnet synchronous motor drive so far discussed [31] has only the speed control loop. It is unstable if there is a large variation of torque due to any reason. The drive can be operated in a more general way by introducing a torque control feedback loop which makes the drive more stable and efficient. Moreover, the drive response can be improved with the introduction of this additional feedback loop. The block diagram of this modified drive is shown in Fig. 4.13. The functional descriptions of different loops of the block diagram have already been discussed in the previous section. Here, an additional PI controller is used to obtain the reference torque after the comparator. The generated torque expression can be written as [41]

$$T_e = \frac{3}{2} \frac{P}{2} \lambda_M i_q^* \quad (4.17)$$

The feedback torque is calculated by using this expression and compared with the reference torque. The compared signal is applied to another PI controller known as torque controller, the output of which is the reference i_q^* . Once this current is obtained, the drive works in a similar way as the previous one.

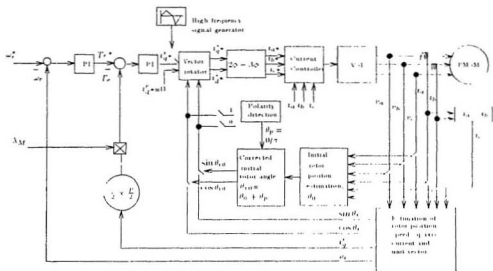


Figure 4.13: Block diagram of PMS motor drive system with two control loops.

The flow chart of the computer simulation of this modified drive is shown in Fig. 4.14. Starting with input data and an initial speed, unit vectors and the torque component current, the subsequent speeds, torque and unit vectors are calculated by the sensorless algorithm. The estimated speed and torque are compared with the reference speed and torque respectively. Using some PI controllers, the inputs of current controllers are generated. The current controllers drive the inverter. The modified drive system is simulated with the following constants for the PI controller: $K_1 = 0.1$, $K_2 = 50$, $K_3 = 0.05$, $K_4 = 200$. The sampling frequency is 10000 Hz. The reference speed taken for this drive simulation is the base speed. Figs. 4.15 to 4.19 show the simulated reference speed, rotor speed, rotor position, unit vectors, phase currents, inverter output voltage, reference output torque of the PI controller, generated torque, torque-speed and voltage-speed characteristics respectively. By introducing torque control loop in the modified drive, the speed response has been improved as shown in Figs. 4.9 (b) and 4.15 (b), respectively. The generated torque loop is now available which is absent in the previous drive. The variation of the torque is compensated by comparing the generated torque with reference torque and using another PI controller. Thus, the responses of the previous system can be improved with the additional cost of PI controllers and comparators.

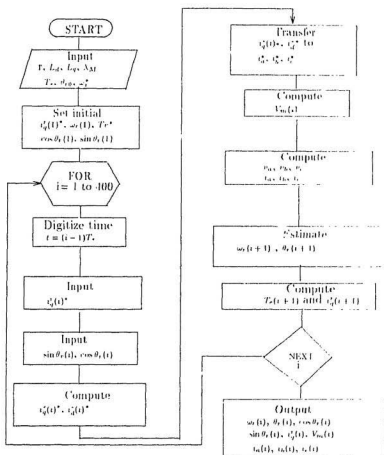
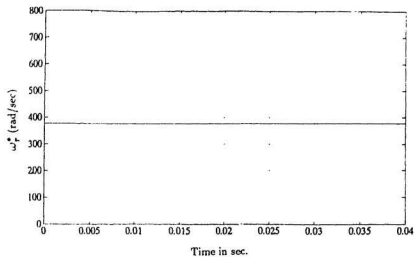
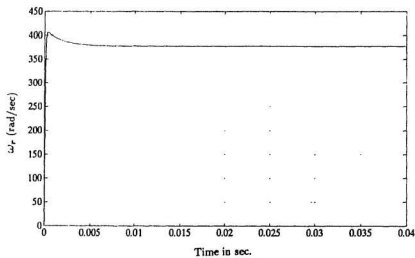


Figure 4.14: Flow chart for the computer simulation of modified PMS motor drive.



(a)



(b)

Figure 4.15: Simulation of two-loop (speed and torque) PMS motor drive. (a) Reference speed. (b) Actual speed.

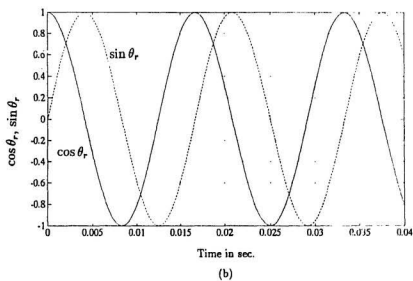
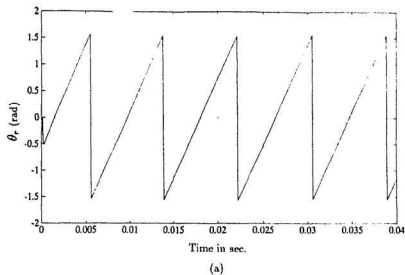


Figure 4.16: Simulation of two-loop (speed and torque) PMS motor drive. (a) Rotor position angle. (b) Unit vectors.

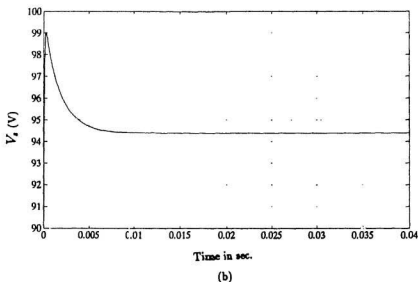
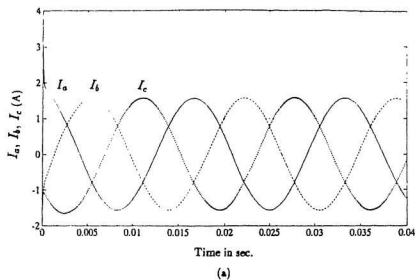
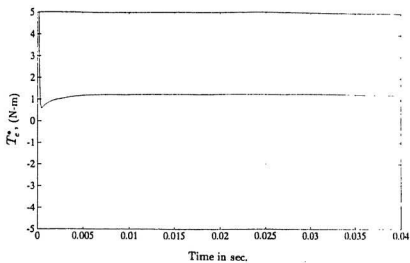
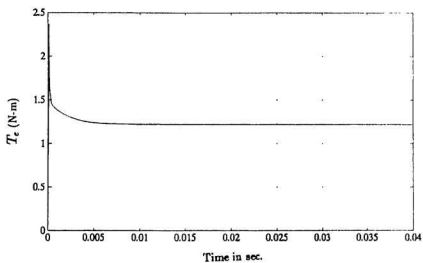


Figure 4.17: Simulation of two-loop (speed and torque) PMS motor drive. (a) Phase currents, (b) inverter output voltage.



(a)



(b)

Figure 4.18: Simulation of two-loop (speed and torque) PMS motor drive. (a) Reference torque. (b) Generated torque.

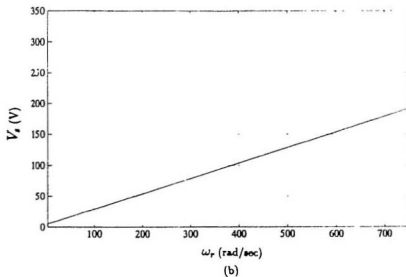
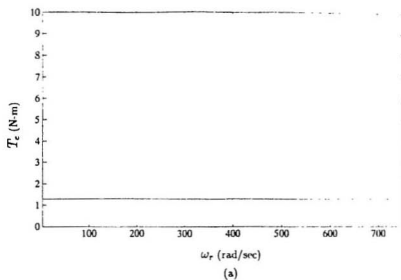


Figure 4.19: Simulation of two-loop (speed and torque) PMS motor drive. (a) Torque vs speed characteristics. (b) Voltage vs speed characteristics.

4.4 PMS motor drive operation above base speed- Field weakening method

The generated or back emf of a permanent magnet synchronous motor is expressed by the following equation:

$$V_b = j\omega_r \lambda_M \quad (4.18)$$

where ω_r is the rotor speed in electrical radian/sec, λ_M is the constant flux produced by the permanent magnet rotor. As the rotor speed increases, back emf increases in a linear fashion since the excitation flux is constant due to the permanent magnets. Thus to reach a desired speed, the terminal voltage must be increased to overcome the back emf. This phenomenon is observed clearly in Fig. 4.19. It is shown in Fig. 4.19 that in order to obtain twice the rated speed, the terminal voltage has to be increased to almost twice the terminal voltage at the rated speed. If it is assumed that the inverter is capable of supplying the required voltage by PWM operation up to base speed ω_b , then an indirect flux control method known as field weakening method may be applied to the drive, so that the terminal voltage will be constant after the base speed. As previously mentioned, owing to the permanent magnet construction of the rotor, nothing can be done on the rotor side from the control point of view. It is possible to weaken the field by controlling the stator current in such a way that a direct axis current component in the rotating frame axis can be generated which will oppose the main field produced by the permanent magnet. The position of this current and the resultant terminal voltage are shown in the vector diagram (Fig 4.20). Hence the expression for V_s is modified as:

$$V_s = (r + j\omega_r L_s)jI'_q + j\omega_r L_s I'_d + j\omega_r \lambda_M \quad (4.19)$$

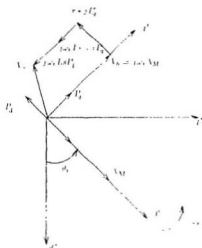


Figure 4.20: Vector diagram of PMS motor above base speed.

The demagnetizing current i_d^* can be generated by introducing an integrator in the drive as shown in the block diagram (Fig. 4.21) where the reference maximum value V_s^* is compared to the generated V_s and the error signal is applied to an integrator. The expression of the demagnetizing current is obtained in the following way:

In Laplace domain, it can be written that

$$(V_s^* - |V_s|(s)) \frac{K_3}{s} = i^*(s) \quad (4.20)$$

In difference equation form, it can be written as

$$(V_s^* - |V_s|(k)) K_3 = \frac{i_d^*(k+1) - i_d^*(k)}{T_s}$$

Or,

$$i_d^*(k+1) = (V_s^* - |V_s|(k)) K_3 T_s + i_d^*(k) \quad (4.21)$$

Where T_s is the sampling period and $k+1$, k are the subsequent sampling instants. The components of the block diagram are the same as in Fig. 4.13 except for an additional branch known as the integrator block $\left[\frac{h_s}{s}\right]$. Its purpose is to obtain the demagnetizing current above the base speed. The computer simulation for this compact drive is done in such a way so that it can be operated at any speed (i.e. above or below the base speed). The flow chart is shown in Fig. 4.22. The values of the constants for PI controllers and the integrator are given as follows:

$K_1 = 0.1$, $K_2 = 20$, $K_3 = 0.05$, $K_4 = 200$ and $K_5 = 10$. It is to be noted that below the base speed, the inverter voltage varies linearly with speed and constant torque operation is obtained in the speed range $0 \leq \omega_r \leq \omega_b$. Above the base speed, the inverter voltage is constant and torque decreases. The simulation results are obtained for twice the rated speed although the drive is capable of operating at any speed. Torque-speed and voltage-speed characteristics are obtained from zero speed to twice the rated speed. Figs. 4.23 to 4.28 show the reference speed, rotor speed, rotor position, unit vectors, phase currents, reference torque, generated torque, torque component current, flux component current, torque-speed and voltage speed characteristics, respectively. This drive system is capable of operating at any speed giving

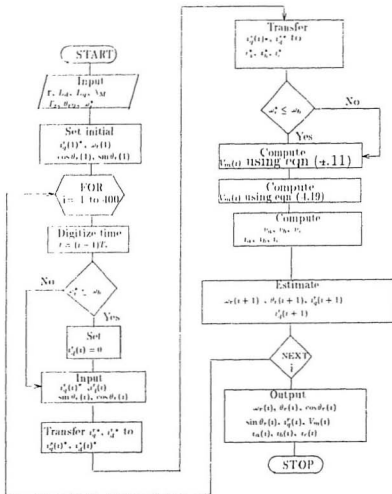


Figure 4.22: Flow chart for the computer simulation of PMS motor drive-operated at any speed.

smooth torque and speed as shown in Fig. 4.28. The speed response problem in drive with only speed loop has been minimized in this complete drive by introducing an additional torque loop, same as in modified drive (Fig. 4.13). But the modified drive cannot be operated above the base speed because of the ceiling of inverter voltage. This problem has been overcome by maintaining the ceiling voltage of the inverter above the base speed by the field weakening method as shown in Fig. 4.28. The rotor position and the unit vectors obtained for this position sensorless drive are relatively noise free as shown in Fig. 4.24 which ensures smooth operation of the hysteresis current controller and voltage source inverter.

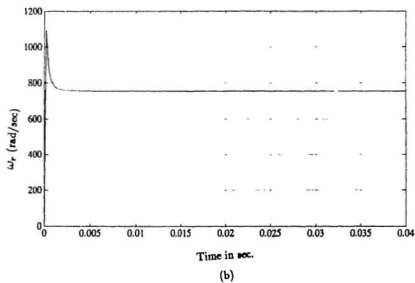
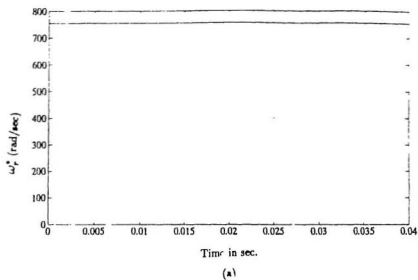


Figure 4.23: Simulation of general PMS drive operated at various speeds. (a) Reference speed. (b) Actual speed.

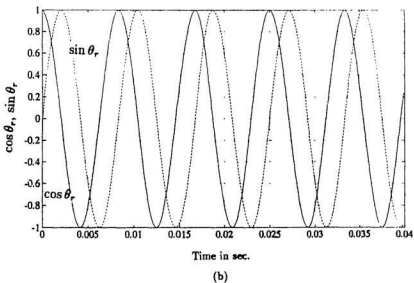
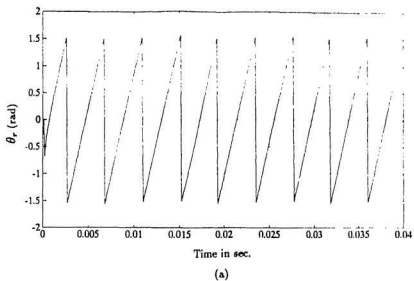


Figure 4.24: Simulation of general PMS drive operated at various speeds. (a) Rotor position. (b) Unit vectors.

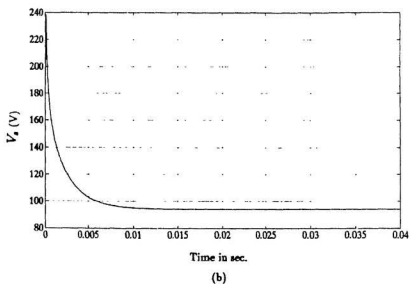
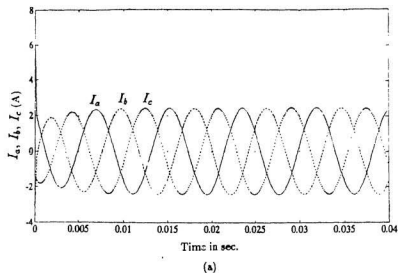


Figure 4.25: Simulation of general PMS drive operated at various speeds. (a) Phase currents. (b) Peak voltage of the inverter.

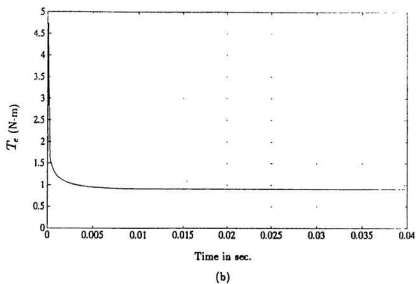
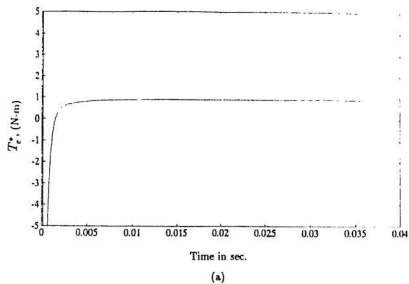


Figure 4.26: Simulation of general PMS drive operated at various speeds. (a) Reference torque. (b) Generated torque.

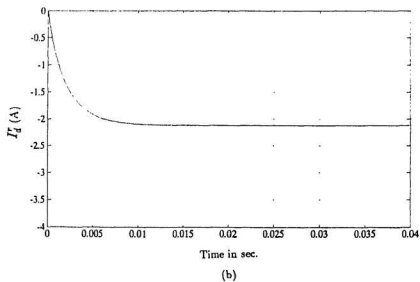
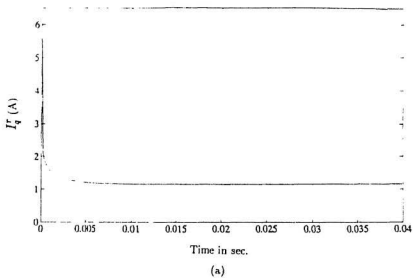


Figure 4.27: Simulation of general PMS drive operated at various speeds. (a) Torque component current. (b) Demagnetizing current.

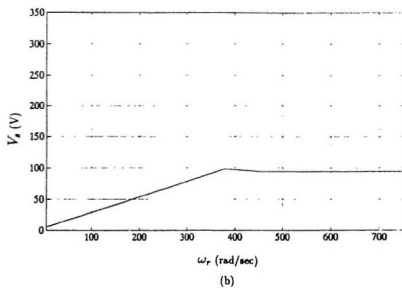
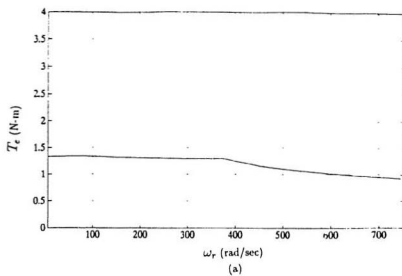


Figure 4.28: Simulation of general PMS drive operated at various speeds. (a) Torque vs speed characteristics. (b) Voltage vs speed characteristics.

4.5 Discussions on Simulated Results

The results of open loop simulation of the PMS motor (Fig. 4.3) give information about the speed ω_r and rotor position angle θ_r . To obtain a variable speed PMS motor drive, it is necessary to have a closed loop operation. The other advantage of closed loop operation is that it is able to account for any parameter variations and also any unwanted external noise. For variable speed PMS motor drive, desired speed is used as reference or command speed and loading effect is not of primary concern. The magnitude of the armature current or power output of the drive mainly depends on the desired reference speed.

Keeping the above facts in mind, simulation has been carried out using speed in the feedback loop at first. Different responses (e.g., rotor speed, rotor position angle, unit vectors, armature current, reference torque component current and inverter output voltage) have been presented in Figs. 4.9 to 4.12. It has been found that after several oscillations in the transient period, the speed becomes constant and the rotor position angle responds according to the speed. Armature currents, unit vectors, reference torque component current and inverter output voltage have also been affected from transient oscillations. Incorporation of another feedback loop (torque loop) makes the drive essentially more stable. The responses have also been improved in the transient period as can be seen from Figs. 4.15 to 4.18. For this configuration the drive has been simulated with different reference speeds (from 0 to twice the rated speed). The torque vs. speed and voltage vs. speed characteristics have been shown in Fig. 4.19. It has been observed that in order to obtain twice the rated speed, the inverter voltage has to be doubled of its rated value. The problem has been solved by introducing the field weakening method. The simulation result with field weakening method in Fig.

4.28 shows that the inverter voltage increases linearly upto the base speed and then remains constant for the subsequent speed.

The sampling frequency for the simulation has been taken to be 10 KHz. Real time implementation of this type of drive is possible with sampling frequency in the kilo-hertz range by using dsp board [27].

Chapter 5

Experimental Results

For the successful operation of position sensorless PMS motor drives, the simulated rotor position angle and rotor speed need to be verified experimentally before the implementation of the control scheme. For this purpose, a laboratory prototype permanent magnet synchronous (PMS) motor has been operated with a balanced set of sinusoidal voltages and parameters used in the sensorless algorithm have been measured. Using the measured parameters, the simulated results of the PMS motor drive using sensorless algorithm for the open loop condition have been verified. The design data of the experimental PMS motor is given in Appendix A.

5.1 Determination of the magnet constant, λ_M

In the sensorless rotor position and rotor speed estimations (equations (3.174) and (3.176)), the magnet constant of the PMS motor, is one of the parameters which needs to be carefully determined. The rotor of the experimental PMS motor used is the Neodymium Boron Iron (NdBFe) permanent magnet. The B-H curve of the NdBFe magnets in the second quadrant is a straight line. Thus the magnet constant

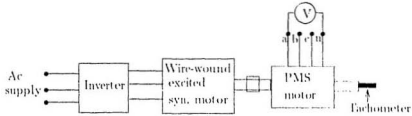


Figure 5.1: Experimental set up for the determination of magnet constant λ_M .

can be found from the following linear relationship:

$$\lambda_M = \frac{V/\text{phase}}{\omega_r(\text{rad/sec})} \quad (5.1)$$

The following test is performed to determine λ_M . The stator terminals are open and the rotor is rotated at constant speed. The induced emf in the winding is proportional to the magnetic flux. Using the relationship of equation (5.1), λ_M can thus be determined. The above linear relationship holds when flux produced by permanent magnet rotor is considered as the straight line function of magnet constant λ_M for high coercive force permanent magnets like NdBF_e, etc.. But for heavy loading condition of motor, λ_M becomes also dependent on the q-axis current, saturation and other factors as well. However, proposed drive systems are stable with a small variation of λ_M . Hence the linear relationship for λ_M expressed in equation (5.1) can be used for this present work.

The experimental set up for the determination of λ_M is shown in Fig. 5.1. The test PMS motor is coupled with a wire-wound excited synchronous motor. An inverter has been used to drive the driving motor at various speeds and the open circuit voltages at various speeds have been measured at the terminals of the test PMS motor. A tachometer is used to measure the rotor speed. The experimental results are given in

Speed, rpm	230	769	1208	1800	2373	3012
Voltage/ ϕ , volt	9.2	30.3	47.8	71.1	93.9	119.3
λ_M , volt-s/rad	0.27	0.266	0.267	0.267	0.267	0.267

Table 5.1: Open circuit voltage and magnet constant at various speeds of PMS motor.

Table 5.1. The average value of λ_M has been found as

$$\lambda_m = 0.2673 \quad (5.2)$$

The wave shape of the induced voltage for the PMS motor has been shown in Appendix B.

The value of λ_M found in the experiment is approximately constant at every speed. The same experiment has been repeated after running the motor for several hours to check whether there is any variation of λ_M with temperature. No significant variation of λ_M with temperature was observed.

5.2 Verification of rotor position angle and speed using sensorless algorithm

For the vector control of the PMS motor, the speed (ω_r) and the rotor position angle (θ_r) needs to be sensed. The present research deals with mechanical sensorless on line calculation of ω_r and θ_r . For this purpose, expressions of ω_r and θ_r have been derived in chapter-three. The parameters of the expressions for equations (3.174) and (3.176) are found experimentally and using these parameters, the rotor position and rotor speed have been simulated for open loop condition. In addition, the input power,

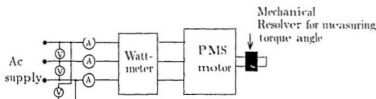


Figure 5.2: Experimental setup for the verification of sensorless algorithm of PMS motor.

phase angle, torque angle have been found theoretically with these experimental parameters. Using the two-wattmeter method, and monitoring the voltage and current wave shapes, the input power and phase angles have been determined experimentally. Steady-state phasor diagram [41] has been used to determine the input voltage of the PMS motor in the drive system. A theoretical torque angle has been found with this vector diagram. A mechanical resolver is used in the determination of the torque angle of the PMS motor in the experiment. The speed ω_r obtained in the experiment is used in the following expression to find the rotor position.

$$\theta_r = \int_0^t \omega_r(t) dt + \theta_r(0) \quad (5.3)$$

The laboratory setup for the verification of theoretical results of the sensorless algorithm is shown in Fig. 5.2.

Sinusoidal voltage is applied to the terminals of the PMS motor. Three ammeters are connected in series in the three phases of the PMS motor to determine the phase currents. Two-wattmeter method is used to determine the input power of the motor. A multi-channel storage oscilloscope is used to monitor the wave shapes of the input voltage and current in order to determine the phase angle. A disk is mounted on the shaft of the motor which gives the direct axis position of the rotor. A position

PMS motor	Input power	Ph. angle, γ	Torq. angle, δ	Speed, rpm
Simulation	62	83.6°	26°	1810
Experiment	66	80.1°	29°	1800

Table 5.2: Simulation and experimental results of open loop PMS motor.

t, msec	0	5	10	15	20	25	30	35	40
Sim. θ_r in deg	0.0	-75.5	32.4	-39.5	68.4	-3.5	-75.5	32.4	-41.7
Expt. θ_r in deg	0.0	-72.0	36.0	-36.0	72	0	-72	36	-36

Table 5.3: Simulation and experimental rotor position, θ_r of open loop PMS motor.

sensor mounted on a reference phase of the stator detects the zero crossing of the induced voltage. Thus the phase displacement between the applied voltage and induced voltage is recorded which is the torque angle of the motor. The speed of the motor is obtained by using a tacho-generator and is displayed on the oscilloscope. The simulation and test results are tabulated in Table 5.2. Simulation and experimental results for the rotor position angle are tabulated in Table 5.3. Fig. 5.3 shows the simulated and experimental rotor position. The plots of the experimental phase angle and torque angle obtained from the oscilloscope are given in Appendix A.

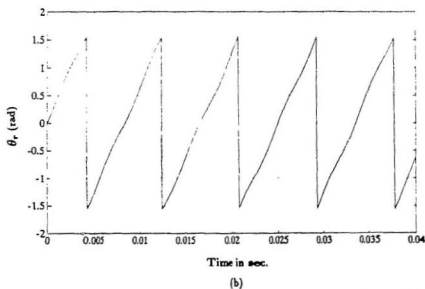
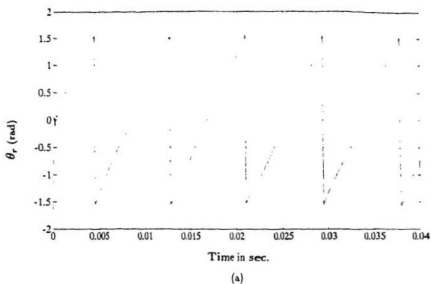


Figure 5.4: Simulated and experimental results of open loop PMS motor: (a) Simulated rotor position angle (b) Experimental rotor position angle.

5.3 Discussions on the experimental results

The concept of using steady-state phasor diagrams to determine the input voltage of the drive system is appropriate as the torque angle found with this phasor diagram is almost the same as that found experimentally. Thus, in the drive system, the input voltage of the PMS motor can be calculated using equation (4.11) rather than using additional sensors. This will not only simplify the system but will make it less bulky. The theoretical value of θ_r concurs with the experimental value of θ_r , thus implying that on-line calculation of rotor position angle can be used in the practical drive system. Based on experimental evidence, it can be concluded that the sensorless algorithm developed is very accurate and can be used for the control of PMS motors. In practice, a fast digital signal processor is used to implement this algorithm. The experimentation with TMSEVM30 digital signal processor for the control of PMS motor is under process at the Power Electronics laboratory of Memorial University. This part is beyond the stated scope of the present investigation.

Chapter 6

Conclusions

This thesis explores the role of the PMS motor in drive systems. Vector control strategy has been considered for the operation of the motor. This method requires information regarding the speed and position of the rotor. Eliminating the requirement of mechanical sensors, this work develops an algorithm for on-line calculation of the rotor speed and rotor position from the knowledge of phase voltages and phase currents. Previous works used voltage sensors to measure the phase voltage. In this work however, calculation of input voltage is provided. It eliminates the need of voltage sensors.

Chapter two investigates various schemes of rotor position detection. Computation based rotor position detection has been chosen for this work. In chapter three, general machine theory is analyzed at first and then Park's machine model has been documented. Using axes transformation theorem, rotor speed and rotor position formulae have been derived in terms of machine parameters, phase voltages and phase currents. In chapter four, computer simulations have been performed for various configurations namely open loop PMS motor, PMS drive with one feedback loop (speed loop) and two feedback loops (speed and torque loops). Based on the results of the

simulations, it can be concluded that the two-loop drive exhibits a better transient response than the one-loop drive. Incorporation of the torque feedback signals in two-loop drive systems would be able to compensate for any instability which is likely to arise due to the abrupt change of load - a problem which is inherent in single loop drive. For variable speed ac motor drives, problems always arise when the motor runs above the base speed, because the inverter voltage needs to be increased by an equal amount to balance the back emf which is proportional to the speed. Field weakening method has been used in this work to operate the motor above the base speed so that the inverter voltage remains constant beyond the rated speed. Computer simulation of this drive has also been performed; and the results are in agreement with the theoretical concepts. In chapter five, tests have been performed on the open loop PMS motor and the data obtained from the tests have been used to verify the sensorless algorithm formulae developed in chapter three. Again, the results obtained from the data are in agreement with those obtained from the simulation. The torque angle obtained from the calculation of the input voltage of the motor is in agreement with that obtained experimentally, thus confirming that the operation of a sensorless PMS drive is possible without the physical measurement of the input voltage.

6.1 Recommendations for future research

This thesis primarily focuses on the computer simulation of speed and position sensorless PMS drive systems. The following recommendations have been made for the real time implementation of the proposed drive.

Since the work deals with the computation based rotor position detection technique for the vector control of PMS motors, high speed digital signal processor (dsp)

is a tool for the real time implementation of this project. Texas Instrument TM SEVM30 dep is capable of performing floating point calculations with extraordinary computational speed. Thus, it is strongly recommended that this processor be used for future research. Suitably programming the processor, which will eliminate the need for various controllers in the drive system is also recommended. This will in effect greatly enhance the efficiency of the system and make it less expensive.

References

- [1] Kuo, B.C., Lin, W.C. and Goerke, U., "Waveform detection of permanent magnet step motors, part I", *Proceedings of Annual Symposium on Incremental Motion Control Systems and Devices*, 1979, pp. 227-241.
- [2] Hair, V.D., "Direct detection of back EMF in permanent magnet step motors", *Proceedings of Annual Symposium on Incremental Motion Control Systems & Devices*, 1983, pp. 211-219.
- [3] Kuo, B.C. and Butts, K., "Closed loop control of 3.6" floppy disk drive PM motor by back emf sensing", *Proceedings of Annual Symposium on Incremental Motion Control Systems and Devices*, 1982, pp. 295-308.
- [4] Siefert, W., "Self synchronization of permanent magnet energized stepper motor with detection of position by evaluation of the BEMF", *Proceedings of Motor-CON*, 1985, pp. 25-35.
- [5] Autognini, L., "Dynamic torque optimisation of a step motor by back emf sensing", *Proceedings of Annual Symposium on Incremental Motion Control Systems and Devices*, 1985, pp. 293-303.

- [6] Iizuka, K., Uzuhashi, H., Kano, M., Endo, T. and Mohri, K., "Micro computer control for sensorless brushless motor", *IEEE Trans. on Industry Applications*, Vol. IA-21, No.1, May/June, 1985, pp. 595-601.
- [7] Antognini, L., "Self synchronisation of PM step and brushless motors A new sensorless approach", *Proceedings of Annual Symposium on Incremental Motion Control Systems and Drives*, 1990, pp. 237-242.
- [8] Becerra, R.C., Jahn, T.M. and Elshani, M., "Four quadrant sensorless brushless ECM drive", *Conference Proceedings of the Sixth Annual Applied Power Electronics Conference* Dallas, Texas, 1991, pp. 202-209.
- [9] Bahlmann, J.P.M., "A full-wave motor drive IC based on the back EMF sensing principle", *IEEE Trans., Consum., Electron.*, Vol.35, No.3, August, 1989, pp.415-420.
- [10] Aarnley, P.P., Hill, R.J. and Hooper, C.W., "Detection of rotor position in stepping and switched motors by monitoring of current wave form", *IEEE Trans. on Ind. Electron.*, Vol. IE-32, No.3, August, 1985, pp. 215-222.
- [11] Amaratunga, G., Kwan, K.W., Tso, M., and Crawley, D., "A single chip CMOS IC for closed loop control of step motors", *IEEE Trans. on Ind. Electron.*, Vol. 36, No.4, November 1989, pp. 539-544.
- [12] Panda, S.K. and Amaratunga, G., "Switched reluctance motor drive without direct rotor position sensing", *Conference record of 1990 IEEE Ind. Appl. Soc. Annual Meeting*, 1990, pp. 525-530.

- [13] Frus, J.R. and Kuo, B.C., "Closed-loop control of step motors without feedback encoders", *Proceedings of the 5th Annual Symposium on Incremental Motion Control Systems and Devices*, Urbana, IL., 1976, pp. 1-11.
- [14] Kuo, B.C., "On current detection in variable-reluctance step motors", *Proceedings of the 6th Annual Symposium on Incremental Motion Control Systems and Devices*, Urbana, IL., 1977, pp. 205-220.
- [15] MacMinn, S.R., Rzesos, W.J., Szczesny, P.M. and Jalus, T.M., "Application of sensor integration techniques to switched reluctance motor drives", *Conference record of 1988 IEEE Ind. Appl. Soc. Annual Meeting*, 1988, pp. 581-588.
- [16] Harris, W.D. and Lang, J.H., "A simple motion estimator for variable reluctance motors", *IEEE Trans. on Ind. Applications* Vol. 26, No. 2, March/April 1990, pp. 237-243.
- [17] Ehsani, M., Husain, I., Kulkarni, A.B., "Elimination of discrete position sensor and current sensor in switched reluctance motor drives", *IEEE Trans. on Ind. Applications* Vol. 28, No. 1, January/February, 1992, pp. 128-135.
- [18] Kulkarni, A.B. and Ehsani, M., "A novel position sensor elimination technique for the interior permanent magnet synchronous motor drive", *IEEE Trans. on Ind. Applications* Vol. 28, No. 1, January/February, 1992, pp. 144-150.
- [19] Lyons, J.P., MacMinn, S.R., and Preston M.A., "Flux/current methods for SRM rotor position estimation", *Conference record of 1991 IEEE Ind. Appl. Soc. Annual Meeting*, 1991, pp. 482-487.

- [20] Ertugrul, N. and Acarnley, P.P. "A new algorithm for sensorless operation of permanent magnet motors", *Conference record of 1992 IEEE Ind. Appl. Soc. Annual Meeting*, 1992, pp. 114-121.
- [21] Okongwu, E.H., Wilson, W.J. and Anderson "Optimal state feedback control of a microcomputer using an observer", *IEEE Trans. on Power Apparatus and systems*, PAS-97(2), 1978, pp. 594-602.
- [22] Lumsdaine, A., Lang, J.H. and Balas, M.J., "A state observer for variable reluctance motors", *Proceedings of Annual Symposium on Incremental Motion Control Systems and Devices*, 1986, pp. 267-273.
- [23] Lumsdaine, A. and Lang, J.H., "State observer for variable reluctance motors", *IEEE Trans. on Ind. Electronics*, Vol.37, No. 2, April, 1990, pp. 133-142.
- [24] Dhaouadi, R., Mohan, N., Norum, "Design and implementation of an extended Kalman filter for the state estimation of a PMSM", *Digital Control Application with TMS420 Family-Selected Application notes*, Texas Instrument, 1991, pp. 355-362.
- [25] Jones, L.A., and Lang, L.A., "A state observer for the permanent magnet synchronous motor", *IEEE Trans. on Ind. Electronics*, Vol.36, NO.3, August, 1989, pp. 374-382.
- [26] Matsui, N. and Ohashi, H., "DSP based adaptive control of a brushless dc motor", *IEEE Trans. on Ind. Applications*, Vol.28, No.2, March/April, 1992, pp. 448-454.

- [27] Matsui, N. and Shigyo, M., "Brushless dc motor without position and speed sensors", *IEEE Trans. on Ind. Applications*, Vol.28, No.1, January/February, 1992, pp. 120-127.
- [28] Takahashi, I. and Iwata, M., "High resolution position control under 1 sec. of an LM with full digitized method", *Conference Record of the 1989 IEEE Ind. Appl. Soc. Annual Meeting*, 1989, pp. 632-638.
- [29] Bose, B.K. and Szczesny, P.M., "A microcomputer-based control and simulation of an advanced IPM synchronous machine drive system for electric vehicle propulsion", *IEEE Trans. on Ind. Electronics*, Vol.35, No. 4, November, 1988, pp. 560-571.
- [30] Meshkat, S. and Ahmed, L., "Using DSPs in ac induction motor drives", *Digital Control Application with TMS320 Family-Selected Application notes*, Texas Instrument, 1991, pp. 303-306.
- [31] Naidu, M., and Bose, B., "Rotor position estimation scheme of a permanent magnet synchronous motor for high performance variable speed drive", *Conference Record of the IEEE 1992 Ind. Appl. Annual Meeting*, 1992, pp. 48-53.
- [32] Steingrimsson, H. and Astrom, J.K., "DSP implementation of a disk drive controller", *Digital Control Application with TMS320 Family-Selected Application notes*, Texas Instrument, 1991, pp. 239-253.
- [33] Lessnauer, R., Schumacher, W. and Leonhard, W., "Microprocessor controlled ac servo drives with synchronous or induction motors: which is prefer-

- able?", *IEEE Trans. on Ind. Applications*, Vol.22, No.5, September/October, 1986, pp. 812-819.
- [34] Kume, T. and Iwakane, T., "High performance vector controlled ac motor drives: Applications and new technologies", *IEEE Trans. on Ind. Applications*, Vol.23, No.5, September/October, 1987, pp. 872-880.
- [35] Pillay, P., Allen, C.R. and Budhabhathi, R., "DSP based vector and current controllers for a PMSM drive", *Conference Record of the IEEE 1990 Ind. Appl. Annual Meeting*, 1990, pp. 539-544.
- [36] Qian, J. and Rahman, M.A., "Analysis and microprocessor implementation of field oriented control for permanent magnet hysteresis synchronous motor", *Conference Record of the IEEE 1991 Ind. Appl. Annual Meeting*, 1991, pp. 198-203.
- [37] Wu, R. and Slemon, G.R., "A permanent magnet motor drive without a shaft sensor", *Conference Record of the IEEE 1990 Ind. Appl. Annual Meeting*, 1990, pp. 553-558.
- [38] Krause, P.C., "Analysis of Electrical Machinery", *Mc-Graw-Hill Inc.*, 1986.
- [39] Bose, B.K., "Power Electronics and AC Drives", *Prentice-Hall, Englewood Cliffs, NJ*, 1986.
- [40] Trieszenberg, D.M., "Electric Power Systems", *Purdue University*, 1978.
- [41] Vas, P., "Vector Control of AC Machines", *Clarendon Press, Oxford*, 1990.

Appendix A

PMS motor design data

Rated power= 1 hp.

Number of poles = 4

Base speed $\omega_b = 377$ rad/sec.

Magnetic flux $\lambda_m = 0.2673$ volts/rad/sec.

Stator resistance $r_s = 2.5\Omega$.

Stator leakage inductance $L_l = 0.6205$ mH.

q-axis magnetizing inductance, $L_{mq} = 7.86$ mH.

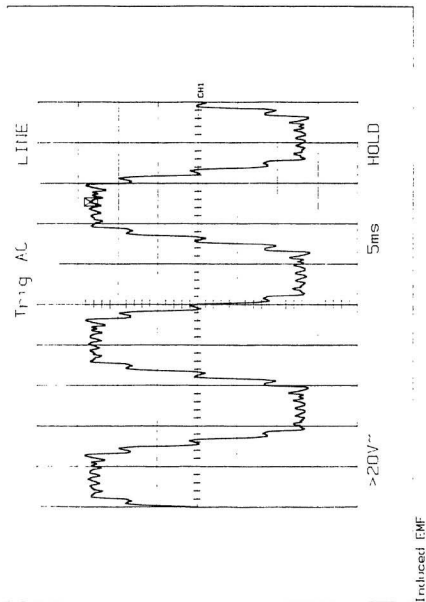
d-axis magnetizing inductance, $L_{md} = 3.33$ mH.

$L_q = L_l + L_{mq} = 8.485$ mH.

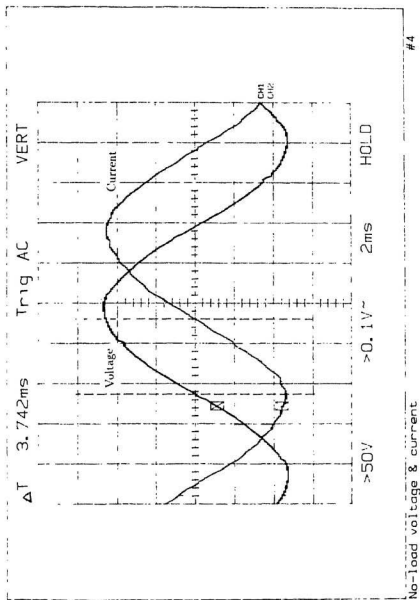
$L_d = L_l + L_{md} = 3.9505$ mH.

Appendix B

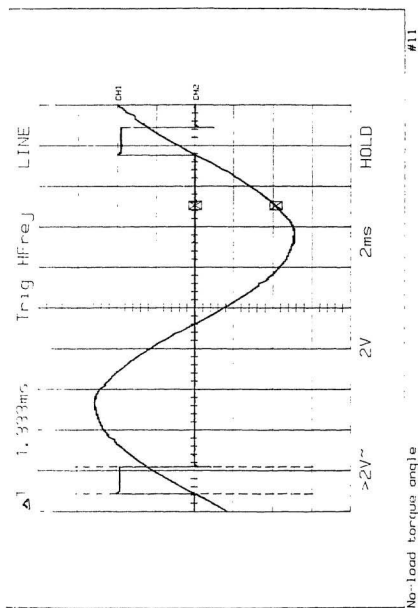
Experimental waveforms



B1: Induced emf by permanent magnet rotor.



B2: Voltage and current wave-form with associated phase angle.



B3: Torque angle measurement

